Grasp Stability with a Robotic Exoskeleton Glove

Teja Vanteddu

Thesis submitted to the faculty of the Virginia Polytechnic Institute and State University
in partial fulfillment of the requirements for the degree of

Master of Science
In
Mechanical Engineering

Pinhas Ben-Tzvi, Chair
Steve C. Southward
Alexander Leonessa

July 24, 2019
Blacksburg, Virginia

Keywords: Exoskeleton, Mechatronics, Grasping, Mechanism, Series Elastic Actuation

Grasp Stability with a Robotic Exoskeleton Glove

Teja Vanteddu

ABSTRACT

Grasp stability was studied and researched upon by various research groups, but mainly focused on robotic grippers by devising conditions for a stable grasp. Maintaining grasp stability is important so as to reduce the chances of the object slipping and dropping. But there was little focus on the grasp stability of robotic exoskeleton gloves and most of the research was focused on mechanical design. A robotic exoskeleton glove was developed as well as novel methods to improve the grasp stability. The exoskeleton glove developed is intended for patients who have suffered paralysis of the hand due to stroke or other factors. The robotic glove aids them in grasping objects as part of daily life activities. The glove is constructed with rigidly coupled 4-bar linkages attached to the finger tips. Each linkage mechanism has 1- Degree of Freedom (DOF) and is actuated by a linear Series Elastic Actuator (SEA). Two methods were developed to satisfy two of the conditions required for a stable grasp. These include deformation prevention of soft objects, and maintaining force and moment equilibrium of the objects being grasped. Simulations were performed to validate the performance of the algorithms. A battery of experiments was performed on the integrated prototype in order to validate the performance of the algorithms developed.

Grasp Stability with a Robotic Exoskeleton Glove

Teja Vanteddu

GENERAL AUDIENCE ABSTRACT

An exoskeleton glove is robotic device that can aid people who suffer from paralysis of their hands caused by a stroke or other factors with the primary goal of allowing them to regain the basic ability of grasping objects and thereby improving their quality of life. The exoskeleton glove developed in this research is focused on objects grasping assistance rather than for rehabilitation purposes. Since the exoskeleton glove lacks conscious senses like a human hand typically possesses, it may not be able to apply sufficient grasping force or may apply excessive force than required irrespective of the object being grasped. In order to ensure that the exoskeleton glove applies the proper amount of force, two novel methods were developed which help improve the overall grasping performance of the robotic glove. These methods use sensors that enable the glove to react to the force interaction changes that exists between the hand and the object being grasped through the exoskeleton glove. The first method detects any deformation that may occur while grasping a soft object and applies lesser force accordingly to prevent further damage to the object. The second method uses motion sensor to detect any movement by the user while grasping the object and applies corrective forces so that the object doesn't slip from the hand. A prototype was designed and integrated and the two methods were tested on the prototype to validate them.

ACKNOWLEDGMENTS

I would like to thank all the people, whose valuable contribution in this field of research has helped me to construct and put forward this work, extending a step further for future research. I would like to thank my advisor, Dr. Ben-Tzvi for the opportunity given to be a part of his lab. His timely guidance and continuous support have always encouraged me to put extra efforts into my work. Finally, I owe special thanks to my family, friends and all the lab members of Robotics and Mechatronics Lab (RML) for their support and strong encouragement over the years of my study and the research. Research reported in this publication was supported in part by the Eunice Kennedy Shriver National Institute of Child Health and Human Development of the National Institutes of Health under Award Number R21HD095027. The content is solely the responsibility of the authors and does not necessarily represent the official views of the National Institutes of Health.

TABLE OF CONTENTS

LIST OF FIGURES

LIST OF TABLES

CHAPTER 1

INTRODUCTION

1.1 Background

An exoskeleton is defined as an orthotic robotic system consisting of links, joints, and/or artificial tendons/muscles, which correspond to that of a human body part. Using the corresponding joints and tendons, the exoskeleton system is able to transmit force/torque and motion through its links onto the joints of the desired body part. Exoskeletons are robotic devices worn by humans which have recently become popular for the great potential in various applications. The application fields include interests from the military, industrial workplace, and medical field. Generally, these robotic systems are worn to provide an enhancement in human strength or to restore movements in limbs that lack motor functionality.

General Electric made initial efforts to create an exoskeleton in 1965 [1]. By partenering with US army and Navy, their device was designed such that it would allow the user to lift a load of 1500 lbs. (680 kg). After the initial step was taken, a lot of research was performed on exoskeletons and numerous types of exoskeleton were developed. These exoskeleton can be broadly classified as Upper extremity exoskeletons and lower extremity exoskeletons. Upper extremity exoskeletons and full-body exoskeletons [2] are popular in the fields of power-assistive devices [3], rehabilitation [4,5], robot-teleoperation, and haptic interaction in virtual reality [4]. Lower extremity exoskeletons on the other hand, serve mainly as rehabilitation and power assistive

devices for those with leg disabilities [6–8]. Hand exoskeletons are classified as a subcategory of upper extremity exoskeletons and will be the focus in this thesis.

Millions of people have trouble in performing activities of daily living (ADLs) such as grasping a bottle, holding tools, eating etc. because of diseases and injuries caused by stroke, cerebral palsy, muscle sprain etc. One particular study states that over 6.7 million people have trouble grasping everyday objects such as a cup or a pencil [9]. Thus hand exoskeletons or exoskeleton gloves were proposed as a possible solution for aiding people with dysfunctionality in their hands and gained research interest within the medical field. One popular application of the exoskeleton gloves was in rehabilitation through which the patient can recover hand strength, grasping capacity by repeated hand exercises. Exoskeleton gloves aided in performing these exercise when worn by the user. In cases where the patient's dysfunctionality was long term and cannot be recovered by rehabilitation, exoskeleton gloves were developed to aid them in grasping objects and ADL.

Soon other applications were found for the exoskeleton gloves which include the field of virtual reality and teleoperation. In the case if virtual reality, the exoskeleton gloves are used to interact with virtual objects by providing haptic feedback and force feedback. They are also explored in the field of teleoperation where it is used as master robot to control a slave robot or device like mobile robot or industrial manipulator.

The exoskeleton gloves to be ergonomic to the user, it has to be compact, lightweight, and efficient. Most of the researchers have focused on solving this problem, so many designs for exoskeleton glove were developed which satisfy one or more of the features mentioned before and one such glove which satisfies most of the features was developed

by Refour et al [10,11] . Even though there was great progress in the field of mechanical design of exoskeleton gloves, there was limited research performed on intelligent grasp control and stability of the grasp. Most of the gloves use very simple grasping methods which may fail in some cases. Most of the times, the glove has very limited knowledge about the object properties and also the motion of the object caused by the user.

Two methods are proposed in this thesis which addresses two of the problems to improve the stability of the grasp. The rest of this chapter will present the research contributions made by this research work. In addition, an outline for the following chapters of the thesis is provided.

1.2 Contributions

In this research, two algorithms were developed which improve the grasp stability and were tested on a glove prototype. The major contributions of the work presented herein are summarized as follows:

1. Deformation Detection algorithm which can detect deformation while grasping soft objects and then adjusts the grasping force accordingly. This algorithm uses minimal number of sensors to sense the deformation and reduces the grasping force in proportion to the deformation detected to prevent further deformation.
2. Optimal force algorithm was developed which generates an optimal set of forces for the four fingers of the glove and also uses information from a motion sensor (9-axis IMU) to adjust the forces based on the orientation and acceleration of the object. The fifth finger which is the thumb finger acts as a support finger which provides reaction force based upon the force applied by the other four fingers. This also

simplifies the algorithm and control of the prototype glove.

3. Designed, manufactured and assembled an exoskeleton glove prototype with optimized linkage mechanism, more robust joints, upgraded thumb joint and faster linear Series Elastic Actuators (SEA). This prototype was used to implement and test the algorithms developed.

1.3 Thesis Structure

A brief overview of the chapters presented in this thesis is presented in this section which is organized as follows:

Chapter 1:

Provides a brief background and presents the main contributions of the thesis

Chapter 2:

Provides a comprehensive literature review and detailed analysis of exoskeleton gloves developed, followed by a literature review of research on grasp stability in robotic grippers and exoskeleton gloves.

Chapter 3:

Problem statement and a motivating application is discussed in this chapter. This discussion defines grasp stability and how the algorithm developed will improve grasp stability.

Chapter 4:

Describes the mechanical design of the exoskeleton glove. Description includes the improvements and upgrades in mechanical design of the linkage mechanism. This section also discusses the sensors and the onboard computation components onboard the glove.

Chapter 5:

Presents the deformation detection algorithm which uses sensor information to adjust force values. The algorithm is implemented in MATLAB on an approximate dynamic model and results are presented. Then, optimal force algorithm which uses information from IMU and SEA while processing is presented. A hardware in the loop simulation is performed and the results are compared with that of a healthy human hand.

Chapter 6:

Presents the experimental setup using the prototype glove and the implementation of the two algorithms discussed in earlier chapters. The results obtained from these experiments are also discussed.

Chapter 7:

Summarizes the work and discusses directions for future work.

1.4 Selected Publications

Disclosure: Contents from these publications were used in this thesis.

Peer-Reviewed Journal Paper

1. **Vanteddu. T**, P. Ben-Tzvi, "Grasp Stability of a Robotic Exoskeleton Glove", ASME Journal of Mechanisms and Robotics. , *In Preparation, Pending Submission*, July 2019.

Peer-Reviewed Conference Paper

1. **Vanteddu, T.**, Sebastian, B., Ben-Tzvi, P., "Design Optimization of RML Glove for Improved Grasp Performance", Proceedings of the ASME 2018 Dynamic Systems and Control Conf. (DSCC 2018), Atlanta, GA, Sep. 30 – Oct. 3, 2018

CHAPTER 2

LITERATURE REVIEW

Exoskeleton gloves are used for various applications including virtual reality, tele-operation, rehabilitation etc. Exoskeleton gloves have significant potential in the medical field which can assist patients suffering from paralysis in their hands due to stroke and other nerve-related diseases to grasp objects in their daily life. So far there has been ample research on exoskeleton gloves which are lightweight, compact and ergonomic to wear. But there has been little progress in intelligent control of exoskeleton gloves. Ideally a glove should be able to grasp an object with minimal input from the user. The following subsections will present reviews of different types of exoskeleton gloves developed so far after which a general review of types of user input to control the glove is discussed. In the final section, research performed on grasp stability in grippers and gloves is described in detail.

2.1 Hand Exoskeleton Classifications

As described in Chapter 1, lot of research has been performed on the mechanical design of the exoskeleton gloves. State of the art gloves developed so far can be broadly classified into two categories, rigid gloves and soft gloves. These gloves are designed for various applications such as for virtual reality, medical applications. This section describes briefly the two categories of exoskeleton gloves by providing few examples for each category.

2.1.1 Traditional Rigid Exoskeleton Gloves

One of the major advantages of rigid exoskeleton gloves it has better grasp configuration as it uses rigid linkages. The rigid linkages are placed along the finger such that the location of the joints of links closely match with joints of finger, thus allowing the rigid links to apply force on the corresponding joints of the human hand [12–20]. The rigid links can be further designed by analyzing the real hand movement such that it replicates the motion of the finger. This makes the grasping action feel more comfortable and natural as it follows the trajectory profile of normal human finger. Three examples of rigid gloves are described and summarized where brief details regarding their design, sensing method and actuator design are explained.

Three-layered sliding spring glove

Traditionally rigid linkages are used but this hand exoskeleton uses a novel actuation method which uses three-layered sliding spring mechanism to perform flexion and extension motion of the finger [21].

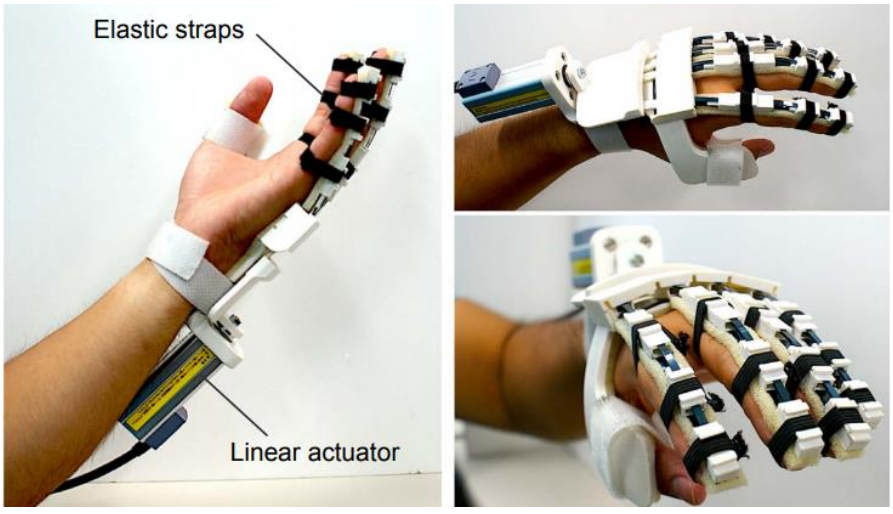

Figure 2.1: Prototypes of the three-layered sliding spring hand exoskeleton [21]

A single motor is used to actuate all the finger mechanisms and can create push and pull motion based on the direction of rotation. The mechanism is designed such that the trajectory of the mechanism matches with natural bending action of the finger. The bending profiles enforced by the glove matched those of the natural flexion/extension joint angles of the human fingers and thumb. Since a single linear motor is used for actuation, control of individual finger is not possible and also due to the large size of the linear actuator, natural Range of Motions (RoM) of the wrist is obstructed. Also there are no force sensing devices on the glove, thus the glove is hard to control while grasping.

Direct driven two-digit hand exoskeleton

This glove consists of a single rigid linkage mechanism for index finger where it is attached on the middle phalange and at proximal phalange in case of thumb [22]. An underactuated revolute-revolute-revolute (RRR) design is implemented as the linkage mechanism.

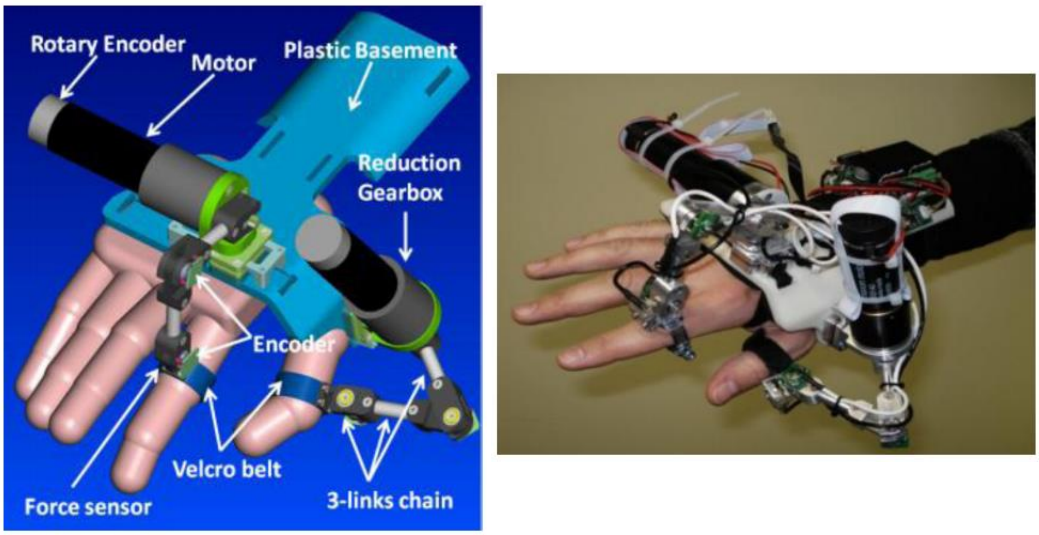

Figure 2.2: CAD design and prototype of the direct drive two-digit hand exoskeleton being worn [22]

This mechanism consists of three serial planar links and it's actuation is achieved by a DC motor. Basic sensory information is provided by position and force sensors and are incorporated within the design. Jerk disturbances created during actuation are minimized by implementing a control scheme. The prototype weighs around 1 kg which is heavy for prolonged use and can cause discomfort to the user. In addition, position feedback is used to control the proposed prototype thus there is no control over forces being applied.

SAFE Glove

The SAFE glove uses a combination of rigid linkages and routed cable actuation to achieve a lightweight, portable design [18,20]. DC motors are used to actuate the cable mechanism and provide about 10N force at the tip of the finger tips.

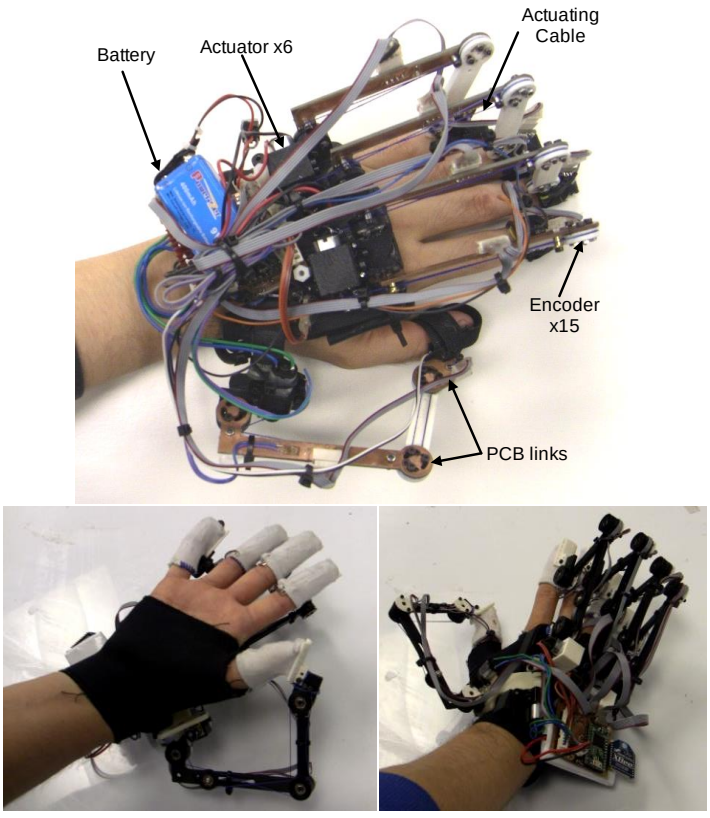

Figure 2.3: Prototypes of the SAFE Exoskeleton Glove: Design II (top) and Design III (bottom) [18], [20]

The weight of the prototype glove is around 430 g. The glove is adjustable for various hand sizes due to the linkage-cable mechanism. Force feedback control is implemented which uses force sensors and also incorporates position sensors.

2.1.2 Soft Exoskeleton Gloves

Soft gloves use softer materials instead of rigid links thus giving them a lightweight and compact design. Two popular methods used for actuation in soft gloves are cables and elastic polymers. Attachments are placed between cable and fingers at specific points so that approximate natural grasping motion is created [23–26]. In the case of elastic polymers, bending action is achieved by inflation of the polymer which can apply force on the fingers and thumb accordingly [27–30]. Brief details of few examples of the soft glove are provided below. Description includes details regarding types of actuation, sensors, features and characteristics of the glove.

Seoul National University (SNU) Pneumatic Hand Exoskeleton

Rigid exoskeletons have the drawback of being heavy and bulky, SNU developed this glove to address the issues faced by rigid gloves. The glove uses pneumatic artificial muscles for actuation of the fingers [27]. Pneumatic artificial muscles are special polymers that bend when inflated thus applying bending motion to the fingers attached. The glove design is simpler, lightweight and compact in size due to the implementation of these artificial pneumatic muscles. A linkage mechanism was used along with the artificial muscles to enable better grasp configuration as obtained in a rigid glove. The total grip force outputted by the glove was 42.2 N when using air pressure of 2.8 bar. The

total weight for the hand exoskeleton was less than 150 g, excluding the pneumatic actuators and air compressors.

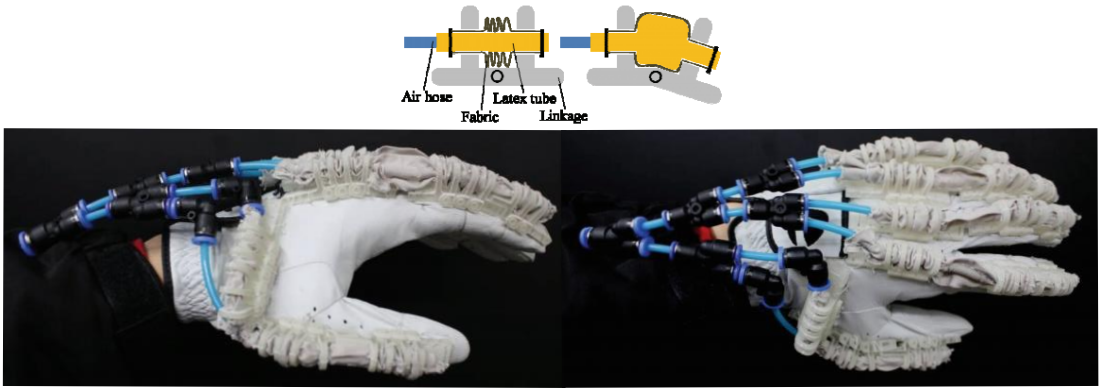

Figure 2.4: Prototype of the pneumatic hand exoskeleton [27]

The pneumatic actuators require air tank or air compressor for it to function,this this hand exoskeleton is not fully portable. In addition to lack of portability, there is lack of controllability of position of fingers or tip force on fingers. Also single pneumatic actuator is used to actuate all the fingers thus applications requiring control of individual fingers cannot use this glove.

BiomHED

The BiomHED is a soft glove that uses exo-tendons which translate to external tendons as they mimic natural tendons. This glove is designed for users with hand impairments [24] and the user can perform distal hand and proximal arm movements. Exo-tendons are made of four cables for each of the fingers which are actuated to control the finger. Tendons are routed through thermo plastic guides placed at specific points so as to produce a coupling relationship between the joints. Seven DC motors with gearhead are used to transmit forces to the exo-tendon system. This actuation system produces around 10 N of force from each actuator and the whole glove including the forearm

bracket and motors weighs around 1 kg. The system does not include encoders with the motors to measure the individual joint angles of the fingers and thumb.

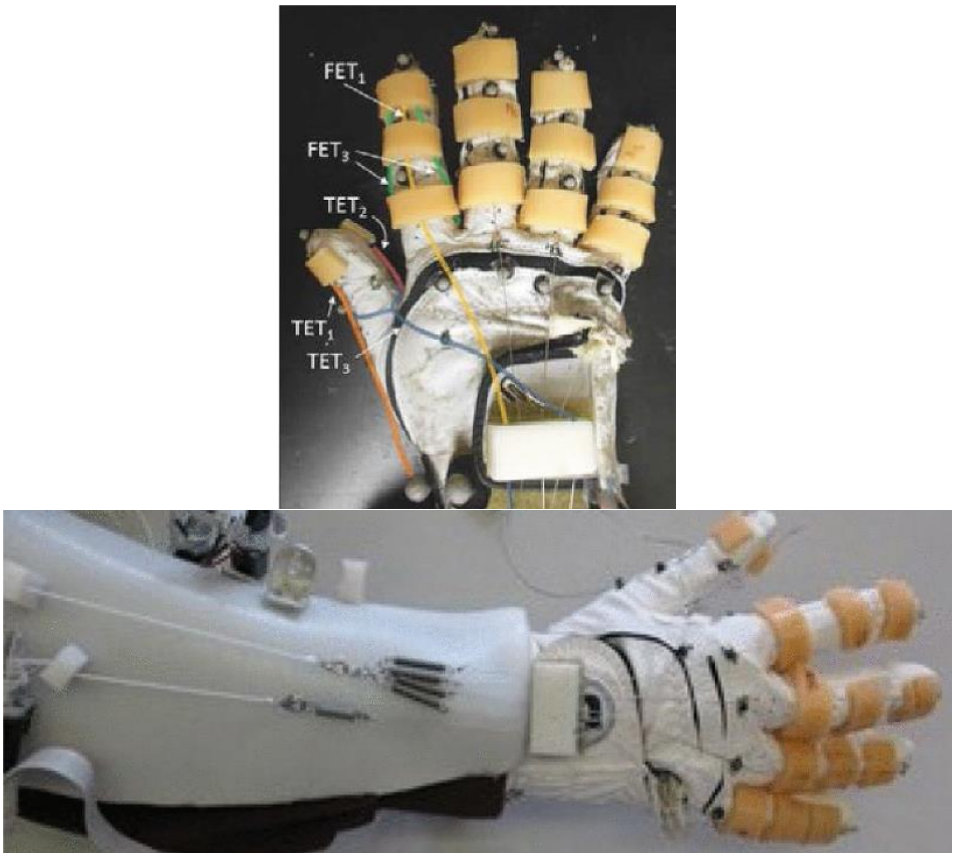

Figure 2.5: Prototype of the BiomHED [24]

The system requires the use of a motion capture system to provide the joint angles as it does not include encoders to measure the joint angles of the fingers.

Exo-Glove

The Exo-Glove is a wearable robotic hand exoskeleton that was designed to be lightweight and compact using a soft tendon routing system [23]. Actuation is implemented only on the index and middle finger and achieves stable grasping. The tendons are bio-inspired and mimic the natural tendons of the finger in terms of transmitting forces. The cable system consisted of three components, as shown in Figure

2.6: (1) thimbles to insert and hold the tip of the finger/thumb, (2) pulleys made of fabric straps that are attached to the phalanges of the finger/thumb and Teflon tubes that were stitched to the fabric to allow for cable routing, and (3) Bowden cables that act as tendons in which one end is connected to the actuation unit and the other to the finger/thumb.

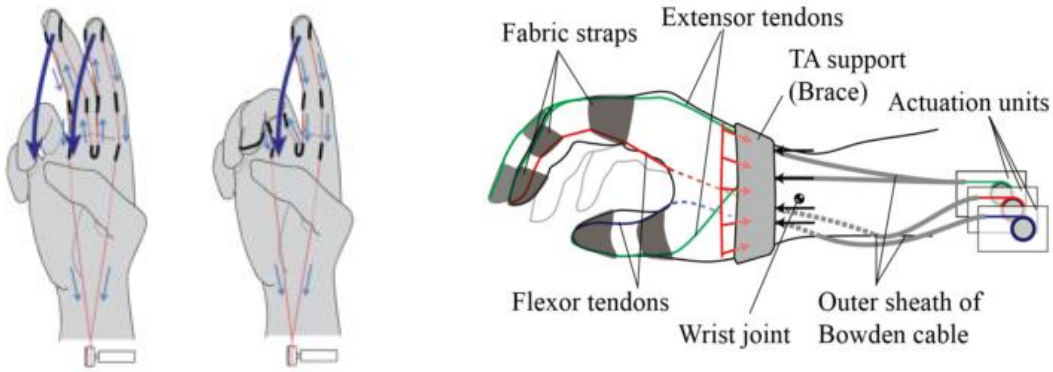

Figure 2.6: Mechanism design for the Exo-Glove [23]

Since there are few fingers to actuate, the glove is unable to achieve othe types of grasps that require all the four fingers. There is no mechanism in place to ensure the coupling between the joints thus the motion of glove is unable to match with natural motion of hand. The use of pulley cables also introduces friction and sheared force from the cables attached to the soft material of the glove being applied.

2.2 Research on Grasp Stability

Any robotic gripper or exoskeleton glove when grasping objects needs to apply sufficient forces such that they satisfy the stability conditions as defined by various researchers, as given in [31–34]. For a grasp to be stable, the forces being applied on the

object should satisfy the force and moment equilibrium, the forces should not be large so as to prevent deformation of the object and damage to the fingers. Other conditions include slip prevention but in this research the focus was devoted to the former two areas mentioned, and algorithms were developed to satisfy these two conditions. Most of the work on stable grasp was implemented for robotic grippers and not for exoskeleton gloves.

The Robotics and Mechatronics (RML) glove needs to use all five fingers for grasping objects as it will reduce the amount of force applied by individual fingers except for the thumb and also reduces the chances of the object from slipping and falling [35]. Some research on grasp stability includes grasp stability learning using tactile information which essentially incorporates sensors all along its fingers. This hand with three fingers has a model which predicts the stability of the grasp based on the tactile information [36]. Akira Nakashima et al have defined conditions for a stable grasps and designed a controller for a single finger that satisfies the stability conditions [32]. Work on stable precision grasps was carried out on a two finger pinch gripper by Kragten et al [37]. Here they made mechanical design changes to a gripper linkage so that the stability increases. Multi-fingered gripper stability analysis was done [38] where they perform stability analysis of a gripper with four fingers on a cube oriented such that the forces on the fingers are symmetric. A parallel hybrid hand was designed by Yi Lu et al [33] where the forces on each finger were determined by optimization so that the forces are as far as possible from the boundary of friction cone, where friction cone is a cone formed by the maximum theoretical friction force vectors about the point of application of force. But this analysis was performed without considering the mass of the object and only the

external forces were taken into account. Maximilian worked on the effect of passive reactions on grippers with stiff and non-back drivable actuators on the stability of a grasp [39]. Yasemin Bekiroglu et al have developed a method to assess grasp stability based on reading from visual and tactile sensors and implemented a learning framework which is trained using synthetic datasets [34]. Most of the research discussed was focused on robotic grippers and there is very little progress in exoskeleton gloves. Sensors were developed for Sensing and Force-Feedback Exoskeleton Robotic (SAFER) glove that could detect slip while grasping an object and iteratively and incrementally increase the gripping forces every time a slip is sensed [40]. Ravi et al developed prediction algorithms that can detect the slight movement in the fingers and predict the type of grasp intended by the user which is executed by the exoskeleton glove to completion [41,42].

In the field of grasping of deformable objects, Ayanna Howard et al [43] have trained a neural network algorithm to extract minimum gripping force required for a deformable object whose deformation characteristics are physically modeled. Another neural network based approach was used by [44] where vision was used to monitor the deformation of soft objects and maps it to the force measured. This information is used in controller to improve the grasp stability of soft objects. A tactile sensor is developed by [45] , whose haptic feedback can be used to differentiate between soft and rigid objects. This sensor can be used on a gripper at the finger tips and the sensor data can be used to apply force based on the soft or rigid object detected. Another method by [46] uses vision sensor and other sensor data like finger position, velocity and force applied, to build 3D model of the object and its deformation. A. Delgado et al have developed a control strategy described in [47] which uses tactile information to adjust its force limits based on the deformability

degree calculated for the object. Grasping of soft objects with flexible tool was studied by [48] where visual information from stereo cameras is used to control the position of the tool tip while making contact with the soft object and neural networks is used to improve the accuracy of the position of the tool.

CHAPTER 3

PROBLEM STATEMENT AND PROPOSED SOLUTION

This chapter focuses on two conditions which determine the grasp stability, which are: (1) Deformation prevention, (2) Optimal force application so as to satisfy the force and moment equilibrium.

When grasping soft objects, exoskeleton gloves don't have any information on the properties of the object. So in case of applying excess force, it may cause damage to the object thus causing inconvenience to the user. Therefore, there is need for the glove to detect such scenarios by itself and subsequently apply corrective actions to prevent further damage to the object. The current RML glove has fewer sensors compared to SAFER or intelligent SAFER (iSAFER) glove. The Force Sensitive Resistors (FSRs) attached to the finger tips to measure the tip force are eliminated. As such, the glove has a more simpler feel, and the user doesn't feel obstructed by sensors. The forces are measured by the SEAs and then using a Jacobian relation, are transformed to tip forces. Solution for detecting deformation is based on the principle that that the soft object, even while deforming, applies a resistive force which is proportional to the stiffness of the material. The glove detects the contact with the object and upon further application of force there is a change in position of the linkage while the SEA is measuring some force. Based on the displacement of the linkage measured by the sensor, the glove can determine the stiffness of the object. The higher the displacement, the lower is the stiffness of the object. This principle is used in the developed algorithm that decreases the reference force to prevent any further damage. The reference force is reduced in proportion to the softness of the object detected by the glove. The details of the

algorithm, simulation results and the experimental results are detailed in subsequent chapters.

The second condition for grasp stability involves the application of optimal forces that satisfy force and moment equilibriums. While grasping an object with certain mass properties, it is required that the glove apply forces such that it satisfies the force and moment equilibriums. If the forces don't meet these equilibrium conditions, then the object may slip or may cause inconvenience to the user holding it because of the unnecessary stresses caused due to application of excessive force. For the sake of simplicity, only cylindrical grasps were considered as they are the most common grasp type in daily life activities. Three points of contact are necessary and sufficient to grasp a 3D object, but while performing cylindrical grasp with the glove, five fingers will be in contact with the object. Since there are more contact points than necessary, there will be infinite combinations of force distributions that can satisfy the force and moment equilibriums. Therefore, an optimization method was used to find the optimal set of force distribution that meets the stability conditions. While grasping the user may move the object in a translational motion or rotational motion or a combination of both. During this user imparted motion, the forces required to meet the equilibrium condition also change in a dynamic manner because of change in orientation or inertial load. Therefore, a motion sensor is used to measure the real-time kinematic state of the glove which is fed into the optimization algorithm to calculate the optimal set of forces. Applying an optimal set of forces not only makes the grasp feel more natural, but also saves power thus enabling longer battery life. This will aid in making the exoskeleton glove to be portable and durable instead of having the user confined to one location where the glove needs to

be supplied with a power source. Detailed explanation on the motion sensor and the optimization method is provided in the following chapters.

CHAPTER 4

MECHANICAL DESIGN

The RML glove developed by Refour et al [10,11] consists of five linkage mechanisms each attached to each of the fingers. Each linkage mechanism is one Degree of Freedom (DOF) mechanism thus requiring only one SEA per linkage mechanism to actuate as shown in Figure 4.1.

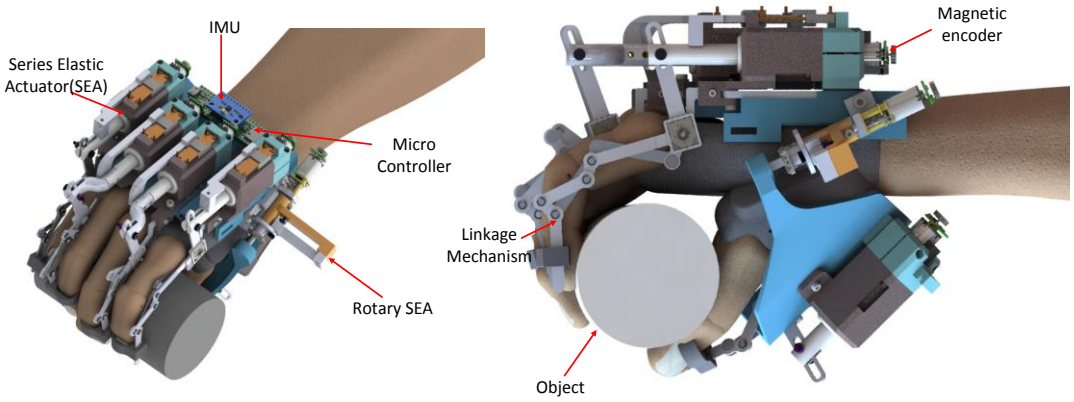

Figure 4.1: Exoskeleton glove worn on a hand to grasp a cylindrical object

The earlier version developed had several drawbacks which were addressed in the improved and optimized design depicted in Figure 4.1 and discussed further in this chapter.

4.1 Linkage Mechanism Optimization

One of the major issues was that the bending angles exhibited by the earlier design were not large enough, thus the glove was not able to grasp smaller objects. It is

important that the glove is able to grasp objects of varying sizes to maximize its usefulness as s glove that can be used in various daily life activities. Design optimization was performed on the linkage mechanism so that the mechanism provides higher bending angles thus enabling it to grasp smaller objects. Upon performing experiments with the previous glove mechanism as part of previous work, results show that the previous glove design cannot grasp objects of width less than 100 mm due to its limited bending angles.

The approach followed includes analysis of the kinematics of the linkage mechanism and selection of proper design variables. The cost function for optimization is formulated so as to maximize the mechanism's ability to grasp objects of varying sizes. Finally, the mechanism was optimized over the design space to find the values of the design variables that maximize the cost function.

4.1.1 Linkage Kinematics

Any optimization problem requires a cost function that needs to be minimized or maximized and design variables to be optimized. Kinematics modelling is performed in order to identify the design variables, the mathematical relation between joint angles, and the design variables. The kinematic modelling of the mechanism was originally conducted in [10] using multi-body modelling techniques. This same model is used to derive the analytical expressions described below. Figure 4.2 presents the kinematic parameters which were used in the analytical expressions.

As shown in Figure 4.2, the various symbols used are l_1, l_2 and l_3 for link lengths, c_1 and c_2 for constraint link lengths, θ_1, θ_2 and θ_3 for joint angles and φ_1, φ_2, φ_3, φ_4 for the angles of constraint joints with respect to the global y-axis.

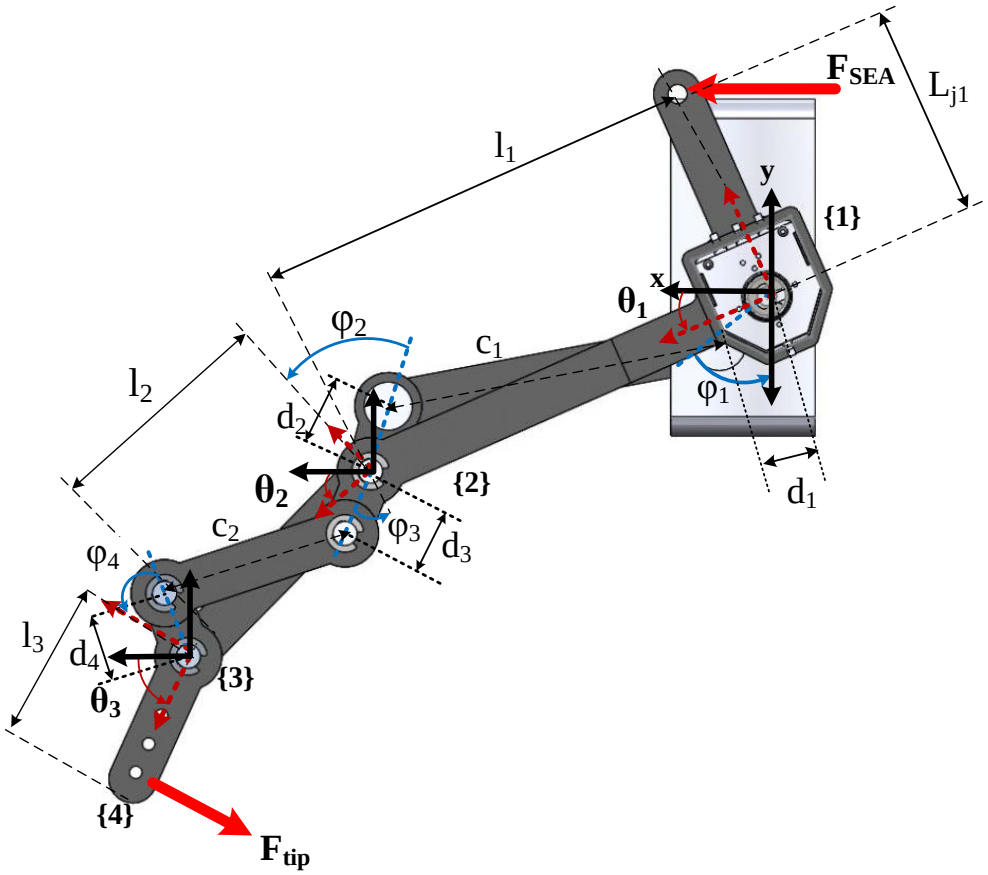

Figure 4.2: Kinematic model of a single finger mechanism

Equation (4.1) and (4.2) relate link parameters as described in Figure 4.2 and angles at each joint.

$$\begin{aligned} c_1^2 = {} & [l_1\cos\theta_1 - d_2\sin\phi_2\cos\theta_2 - d_2\cos\phi_2\sin\theta_2 - d_1\sin\phi_1]^2 \\ & + [l_1\sin\theta_1 - d_2\sin\phi_2\sin\theta_2 + d_2\cos\phi_2\cos\theta_2 - d_1\cos\phi_1]^2 \end{aligned} \tag{4.1}$$

$$\begin{aligned} c_2^2 = {} & [(l_1 + d_3\sin\phi_3\cos\theta_1) - (-d_3\cos\phi_3\sin\theta_1) - l_1\cos\theta_1 \\ & - l_2\cos\theta_2 - (-d_4\sin\phi_4\cos\theta_3) + d_4\cos\phi_4\sin\theta_3]^2 \\ & + [(l_1 + d_3\sin\phi_3\sin\theta_1) - (-d_3\cos\phi_3\cos\theta_1) - l_1\sin\theta_1 \\ & - l_2\sin\theta_2 - (-d_4\sin\phi_4\sin\theta_3) + d_4\cos\phi_4\cos\theta_3]^2 \end{aligned} \tag{4.2}$$

These equations are derived from geometric relations between the linkage parameters. Equations (4.3) and (4.4) are the analytical expressions for θ_2 and θ_3 for a given input angle θ_1, which are derived upon solving Equations (4.1) and (4.2).

$$\theta_2 = \sin^{-1}\left(\frac{B_1C_1 - \sqrt{A_1^4 + A_1^2B_1^2 - A_1^2C_1^2}}{A_1^2 + B_1^2}\right) \tag{4.3}$$

where,

$$A_1 = 2d_1d_2\sin\varphi_1\sin\varphi_2 - 2l_1d_2\sin\varphi_2\cos\theta_1 + 2d_1d_2\cos\varphi_1\cos\varphi_2 + 2l_1d_2\cos\varphi_2\sin\theta_1,$$

$$B_1 = 2d_1d_2\sin\varphi_1\cos\varphi_2 - 2l_1d_2\cos\varphi_2\cos\theta_1 - 2d_1d_2\cos\varphi_1\sin\varphi_2 - 2l_1d_2\sin\varphi_2\sin\theta_1,$$

$$C_1 = c_1^2 - (l_1^2 + d_1^2 + d_2^2 - 2l_1d_1\sin\varphi_1\cos\theta_1 + 2l_1d_1\cos\varphi_1\sin\theta_1)$$

$$\theta_3 = \sin^{-1}\left(\frac{B_2C_2 - \sqrt{A_2^4 + A_2^2B_2^2 - A_2^2C_2^2}}{A_2^2 + B_2^2}\right) \tag{4.4}$$

where,

$$A_2 = 2Bd_4\cos\varphi_4 - 2Ad_4\sin\varphi_4,$$

$$B_2 = -2Ad_4\cos\varphi_4 - 2Bd_4\sin\varphi_4,$$

$$C_2 = c_2^2 - (A^2 + B^2 + d_4^2),$$

$$A = l_1\cos\theta_1 + l_2\cos\theta_2 - ((l_1 + d_3\sin\varphi_3)\cos\theta_1 + d_3\cos\varphi_3\sin\theta_1),$$

$$B = l_1\sin\theta_1 + l_2\sin\theta_2 - ((l_1 + d_3\sin\varphi_3)\sin\theta_1 - d_3\cos\varphi_3\cos\theta_1).$$

These equations can be used to calculate θ_2 and θ_3, provided a known input angle θ_1 and known link parameters l_1, l_2, l_3, d_1, d_2, d_3, d_4, φ_1, φ_2, φ_3 and φ_4. The link lengths have been selected based on previous studies on human hand anatomy as described in [10].

The dimensions were chosen such that they provide a comfortable fit for an averaged size adult male. With these parameters fixed, the optimization will be performed on the following design variables, d_1, d_2, d_3, d_4, φ_1, φ_2, φ_3 and φ_4 for larger values of θ_2 and θ_3.

Apart from objective or cost function and design variables, an optimization problem also includes equality and inequality constraints on the design variables. While performing the optimization, design variables are selected such that they maximize or minimize the objective function and also satisfy any constraints on the design variables.

Since link lengths are fixed, design variables are the remaining link parameters which are d_1, d_2, d_3, d_4, φ_1, φ_2, φ_3 and φ_4. Equations (4.1- 4.2) derived as part of the kinematics modelling are used as non-linear equality constraints. The optimization function used in the previous design was a weighted sum of squared error of joint angles θ_1, θ_2 and θ_3 between the kinematic model and biomechanical data on the trajectory of a human grasp obtained from a study performed by Handcorpus company.

In the earlier design, data from previous medical studies was used to optimize the linkage mechanism. Trajectory of joint angles produced by a healthy human hand was obtained from the data which is used as the target joint angles. This data was selected so that the linkage mechanism will produce similar natural motion. In the process of optimizing this cost function for the complete trajectory, it wasn't able to optimize the linkage to produce large bending angles. Thus, this objective function produces the design variables which produce a trajectory that satisfies the target trajectory on an average.

It can be inferred that the objective function needs to be modified so that the target of producing larger bending angles can be achieved. To meet this target, two objective

functions are formulated and the results are analyzed. Both the objective functions are used in the optimization process to produce design variables and the results are compared to select the objective function with better results.

The weighted sum of the errors for the maximum flexion position of the grasp trajectory between the HUST (Huazhong University of Science and Technology) dataset and the kinematic model is formulated to be the first objective function for this study. As mentioned earlier, link parameters are optimized to produce better θ_2 and θ_3 bending angles for a predefined θ_1 value. This objective function differs from the objective function described from previous work in the fact that it calculates error for only the maximum flexion position.

A study of various grasp taxonomies [49] was used as the source for the joint angles for the desired grasp angles to be used in the optimization. This study describes that there are 33 types of grasps a human performs in his/her daily life depending on the object to be grasped. Among these 33 grasp types, a grasp type which meets the current requirement for high bending angles need to be selected. Two grasps were found to be closest in meeting this requirement which are the lateral grasp (Grasp number 16) and the small diameter grasp (Grasp number 2 in the study). Handcorpus Company performed the study to compile a dataset called the HUST dataset which has the bending angle data for all 33 grasp types performed by 30 subjects. Data for the two grasp types selected was obtained from the HUST dataset. Lateral grasp was found to have higher bending angles as compared to small diameter grasp, so the former grasp is used here onwards for the optimization process. As mentioned earlier, two objective functions are formulated which will be used to produce optimal design variables.

The first objective function for the optimization problem is described in Equation (4.5) where *F(x)* is to be minimized:

$$F(x) = w_1 e_1 + w_2 e_2 \tag{4.5}$$

In the above expression, w_1 and w_2 are the weighting parameters, and e_1 and e_2 are the absolute errors in bending angles θ_2 and θ_3, respectively. Bounds are applied on the design variables such that they meet the design constraints. d_1, d_2 and d_4 have a lower and upper bound at 7 mm and 13 mm, respectively, while d_3 has a lower bound at 6 mm and upper bound at 10 mm. Since d_3 is on the side where the object is being grasped, an upper bound is imposed such that it won't interfere with the object to be grasped. Upper bounds for d_1, d_2 and d_4 are higher than it is for d_3 as these three parameters do not interfere with the object being grasped. To prevent the interference of constraining joints with joint 2 and 3, lower bounds are introduced to the design variables. Upper bound of 80 degrees is applied for the constraint joint angles φ_1, φ_2, φ_3 and φ_4, while a lower bound of 10 degrees is applied to φ_2 and φ_4 variables. Lower bound of 20 and 30 degrees is applied to the design variables φ_1 and φ_3, respectively. The lower bound for the design variable φ_3 is higher than other constraint angles so as to prevent the joint from extending beyond the width of the finger, thus preventing any obstruction while grasping any object due to the mechanism. Since the design variables φ_1, φ_2 and φ4 do not interfere while holding an object, lower bounds for these variables is relatively small compared to φ_3.

As described earlier, a second objective function is formulated as shown in Equation (4.6). Square root of error in distance between the position of tip of linkage as obtained from the HUST dataset and from the kinematic model of the linkage is formulated as the objective function $G(x)$ which needs to be minimized.

$$G(x) = \sqrt{(x_k - x_h)^2 + (y_k - y_h)^2} \tag{4.6}$$

where,

x_k and y_k – Linkage tip coordinates of link l_3 calculated from θ_1, θ_2 and θ_3 obtained from the kinematic model

x_h and y_h - Linkage tip coordinates of link l_3 calculated from joint angles obtained from a specific grasp in the HUST dataset.

Same equality non-linear constraints and lower and upper bounds are applied for the second objective function as well. These two objective functions satisfy the convex function conditions, and as such it becomes a convex optimization problem.

Optimization is performed in MATLAB using *fmincon* function which uses an interior point algorithm to optimize. HUST dataset for the lateral grasp is provided as the target for both objective functions and the results of the optimization are shown in Figure 4.3 where it is compared with the non-optimized case. Compared to the previous non-optimized case, both the optimized results show significant improvement in terms of the bending angle. Quantitative comparison is provided in Table 4.1 between the results of both the objective functions.

From quantitative data from Table 4.1 and observation of Figure 4.3, clearly the second function performs better in achieving the target angles with lower error, so the second objective function is selected for further analysis and optimization of the other linkages. The values of the optimized design variables are {d_1-12.9, d_2-7, d_3-9.4, d_4-7.5 mm}, {φ_1-20.6, φ_2-76.7, φ_3-40.7, φ_4-44.7 degrees}.

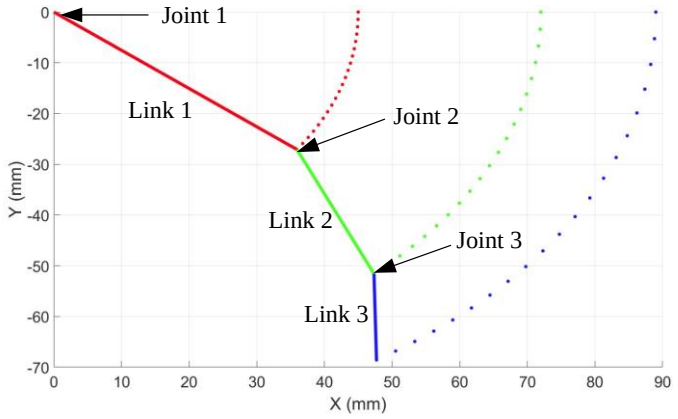

(a)

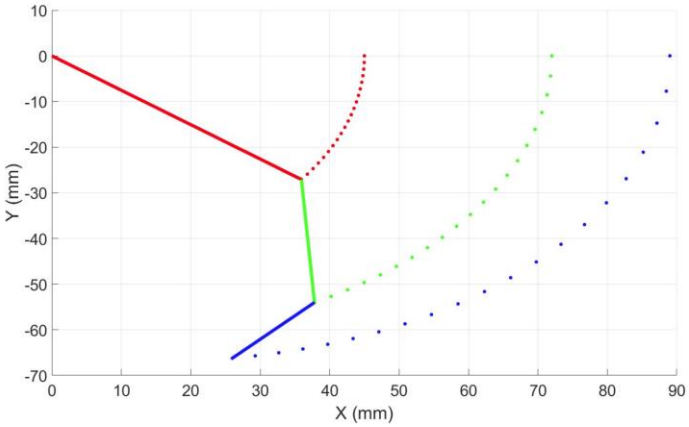

(b)

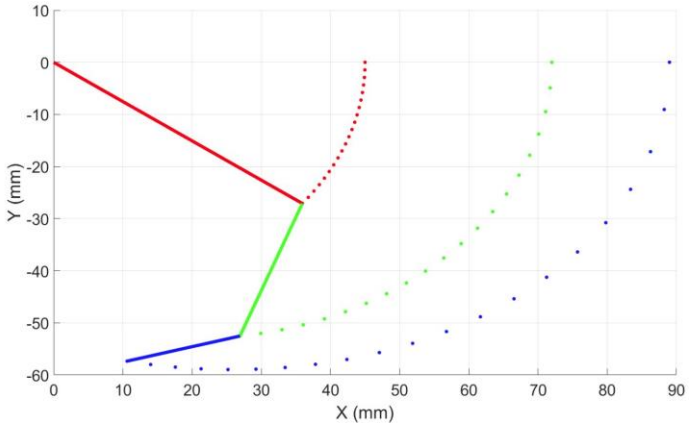

(c)

Figure 4.3: Final position of linkage: (a) Before optimization, (b) After optimization with 1st cost function, (c) After optimization with 2nd cost function

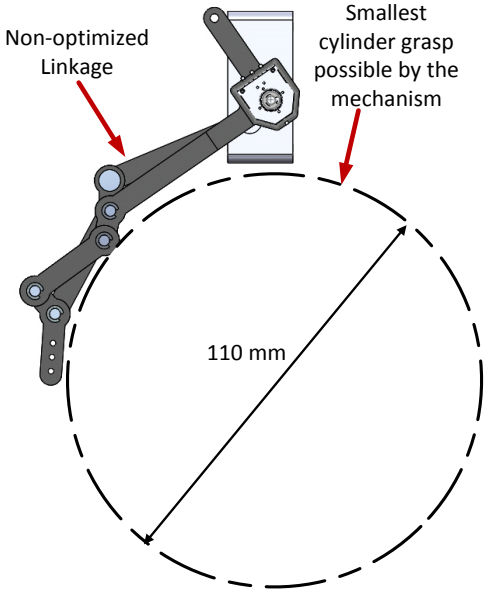

Figure 4.4: Smallest cylinder fit possible for the non-optimized linkage mechanism

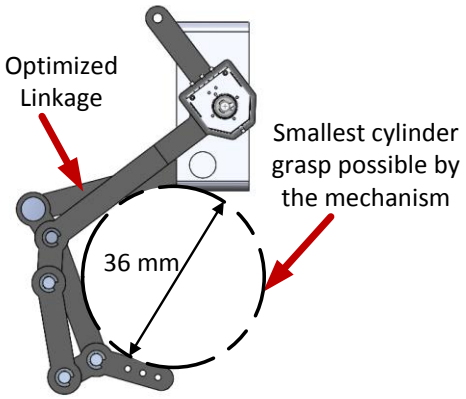

Figure 4.5: Smallest cylinder fit possible for the optimized linkage mechanism

A minimum cylinder is fitted into the linkage to obtain a quantitative improvement as shown in Figures 4.4 and 4.5. Clearly, a smaller diameter cylinder can be grasped when optimized linkage is used as compared to non-optimized linkage.

Table 4.1: Comparison of the two cost functions

	θ_2	θ_3
Target angles (Degrees)	108.2	158.3
Angles achieved with 1st cost function	83.4	130.8
Percent error	-22.9	-17.3
Angle achieved with 2nd cost function	105.7	160.3
Percent error	-2.3	1.3

After this optimization was performed, the same process was repeated for all the other fingers of the glove so that the glove can grasp smaller objects.

4.2 Thumb Mechanism

The thumb mechanism orientation was changed such that the thumb can stretch further and grasp objects with larger dimension. To address this issue, a 3D scan model of a human hand was taken when the thumb is stretched out and is in a grasping position. Then the CAD model of the glove was assembled with the hand. The thumb angle was adjusted by trial and error such that it matches as close as possible to the human thumb. The new thumb orientation allowed it to grasp an object which is around 65 mm in width.

4.3 SEA Design Improvement

In the earlier version, the SEA linear velocity was quite low, leading to a grasp time of 20-30 sec, which is impractical and also the mechanical design was not robust enough. Therefore, a new SEA design was implemented by Ravi et al [50] which uses a different

lead screw thus exhibiting higher linear velocity for the same motor and also is more robust. The new design can flex to its extreme position in 2-3 seconds.

4.4 Mechanical Design Improvements

Earlier version of the RML glove has Adduction/Abduction passive joints to allow the user to move their finger in that direction freely and to avoid any undue stresses on the fingers. This joint was only implemented on two fingers due to design constraints. There was difficulty in rotation of the linkage due to misalignment of the two axes caused due to manufacturing errors. To eliminate this, the design was changed so as to just have one axis of rotation and the actuator also rotates along with the linkage, thus allowing for free motion with minimal obstruction. A shoulder bolt was used as the shaft thus providing robust support to the SEA and the linkage mechanism. This design was extended to all fingers of the glove thus making it more ergonomic to the user.

The connection between the SEA and the linkage mechanism was upgraded to sliding joint type. As the previous version was not robust and upon high force application can invert the mechanism. Also, the Jacobian converting force from the SEA to torque at the first joint of the linkage was complex. By converting it to a sliding mechanism, both issues were solved.

In the previous design version, a rotary potentiometer was used to measure the output of each SEA and the angular position of the linkage mechanism. It was changed to a linear potentiometer as it generates lower noise and provides better resolution, thus improving the accuracy of measurement.

4.5 Rotary SEA Design

Since the whole glove is force controlled using SEAs, there is a need for a SEA for the thumb joint as well. However, it cannot have a linear SEA due to size and design restrictions.

Most of the research on design of Rotary SEA (RSEA) has been mostly too large and heavy [51] for use in glove or they are unidirectional [52], which was not desirable for the current requirements. Therefore, there was a need to design a rotary SEA that is compact, easy to manufacture and doesn't obstruct while grasping objects. After few concept design iterations, a simple beam was used which served as the elastic element. The torque applied to the shaft was transferred to the tip of the beam which bends and creates an angle difference between the shafts.

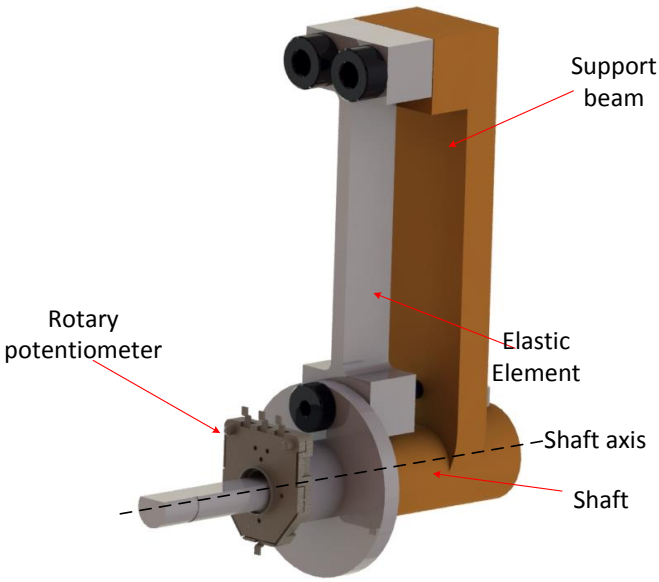

Figure 4.6: Rotary SEA subassembly

The output requirement set for the RSEA was 10 degrees of angular displacement when the glove was holding a 1 kg object and also at this displacement the maximum stress should be less than the yield strength of the respective beam material. The beam has four design parameters which need to be determined such that it meets the output requirements. The four design parameters are length, breadth, height and distance of the tip from the axis of rotation. These four parameters were run through an optimization algorithm in MATLAB to find the optimal values that satisfy the output conditions.

The governing equations relating the torque applied and the angle of deflection is as follows

Where,

$$F_r \cos(\theta_b + \theta_r) R = T_r = m_r g l_m \cos(\theta_0 + \theta_r) \tag{4.7}$$

$$\theta_b = \frac{l}{EI}\left(\frac{F_r \cos(\theta_b) l}{2} + F_r d\right) \tag{4.8}$$

$$\delta = R \sin\theta_r = \frac{l^2}{EI}\left(\frac{F_r \cos(\theta_b) l}{3} + \frac{F_r (d + R - R\cos\theta_r)}{2}\right) \tag{4.9}$$

F_r is the normal force applied on to elastic beam element, θ_b is bending angle of the beam at the tip, θ_r is the bending angle of the shaft, θ_0 is the initial angle of the shaft, m_r is the mass of the object that is used in its testing, l_m is the distance at which object is from the axis of shaft, E is the modulus of elasticity of the elastic beam, I is the moment of inertia of the beam, R is distance between axis of shaft and center of pin applying force on the beam, l is the length of beam and δ is the horizontal distance displaced by the pin.

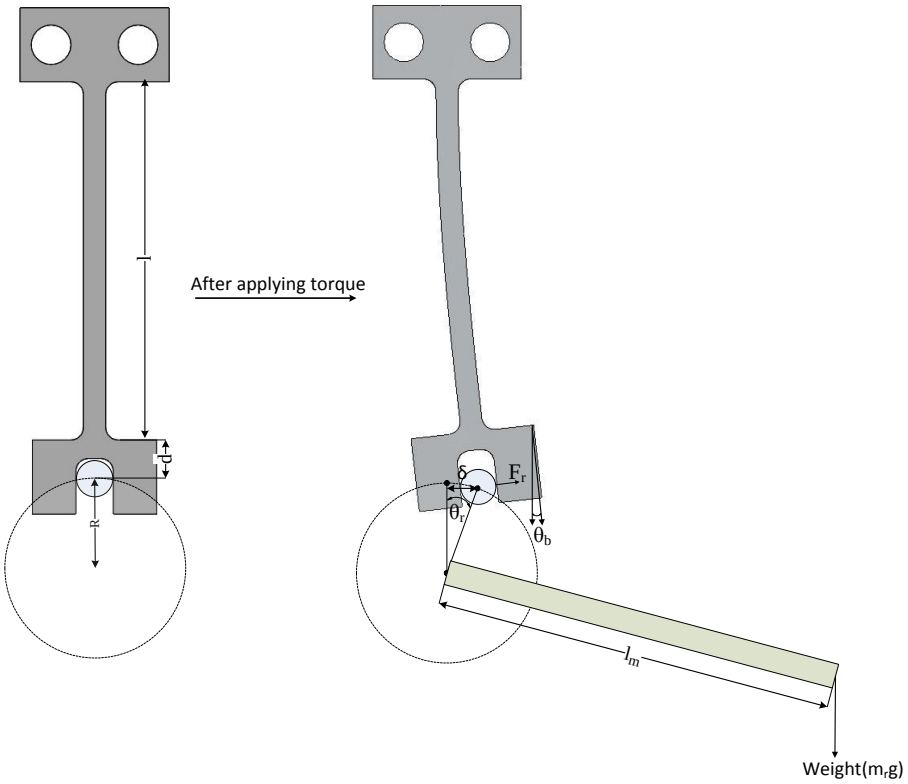

Figure 4.7: Dynamics of the Rotary SEA upon applying force/torque

To experimentally test the RSEA mechanism, a test rig was built where a known load was applied at a known location to generate a torque on the shaft axis. The deflection was then measured using a bourns 3382G rotary potentiometer. The data was read through a teensy 3.6 microcontroller and processed in MATLAB. The experimental plot upon observation was close to a linear relationship. Therefore, a linear equation was curve fitted to the experimental data as given in Equation (4.9). But the analytical data is not closely matching with experimental result which could be attributed to several factors like error in young's modulus, manufacturing errors and friction loss.

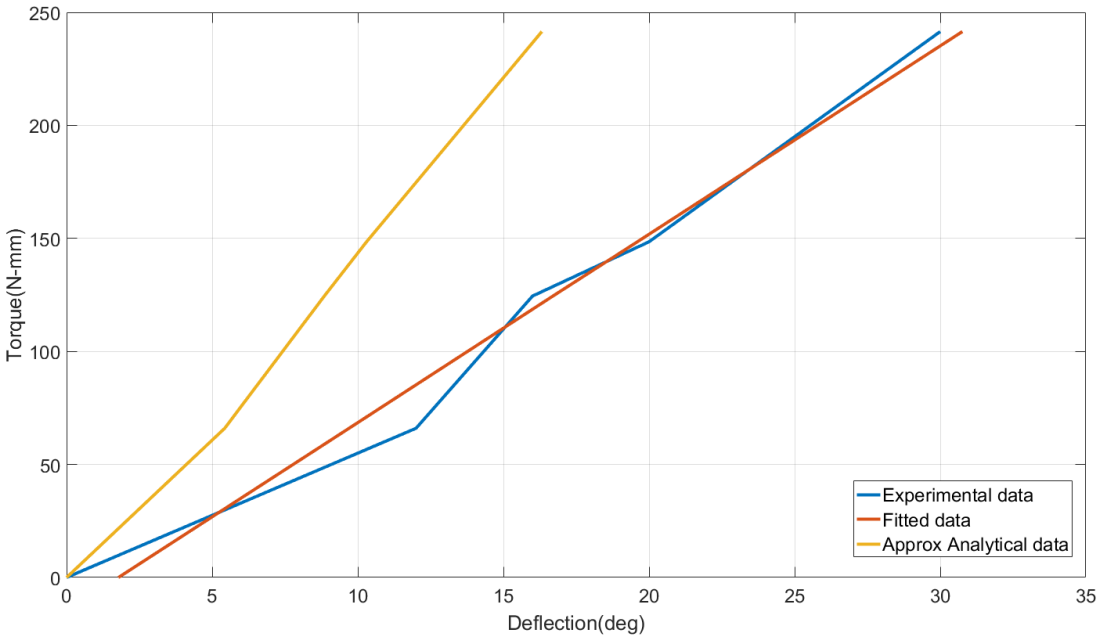

Figure 4.8: Plot comparison of experimental data, fitted data and theoretical solution of RSEA deflection vs. applied torque

4.6 Conclusion

The mechanical design of the RML glove and all the design upgrades were described in this chapter. Major changes included implementation of more ergonomic and optimized linkage mechanism thus enabling grasp of objects with small diameter, robust and faster SEA and a novel Rotary SEA for the thumb joint. Other design improvements included robust adduction joints, use of linear potentiometers, implementation of durable sliding joints for connecting the linear SEA to the linkage mechanism, and upgraded thumb orientation allowing for grasping larger objects.

CHAPTER 5

GRASP STABILITY ALGORITHMS

In order to improve the stability of the grasp of the RML glove, two algorithms were developed which satisfy two of the conditions that include deformation prevention for soft objects and optimal force application so as to satisfy force and moment equilibriums.

5.1 Deformation Detection Algorithm

This algorithm was developed to prevent crushing or deformation of soft objects by the glove. Initially, when the glove is in non-contact state with the object, the user provides intent to grasp the object either by voice command or some input device like an electronic button. Upon receiving the intent to grasp, the linkages of the glove are driven at certain velocity thus closing towards the object. Since the glove doesn't know the shape of the object also due to non-linear relation between the speed of the linear SEA and finger-tip velocity, all four fingers may not touch the object at the same time. If the finger which touches the object earlier than other fingers starts applying force, then it may cause the object to tilt or fall over. To prevent this, the fingers stop immediately upon detecting the presence of an object and wait until all fingers have made slight contact with the object. After ensuring that all the fingers have made contact, the deformation detection algorithm is initialized. This algorithm takes in as input a predefined force that is applied and sent as the reference signal to the actuators. Before the algorithm is further explained, it is important to describe the sensors that are available on the glove necessary for this process. For each finger, there are two sensors, one is a

linear potentiometer and the second is a magnetic hall encoder. The linear potentiometer measures the distance travelled by the end of spring in SEA connected to the linkage.

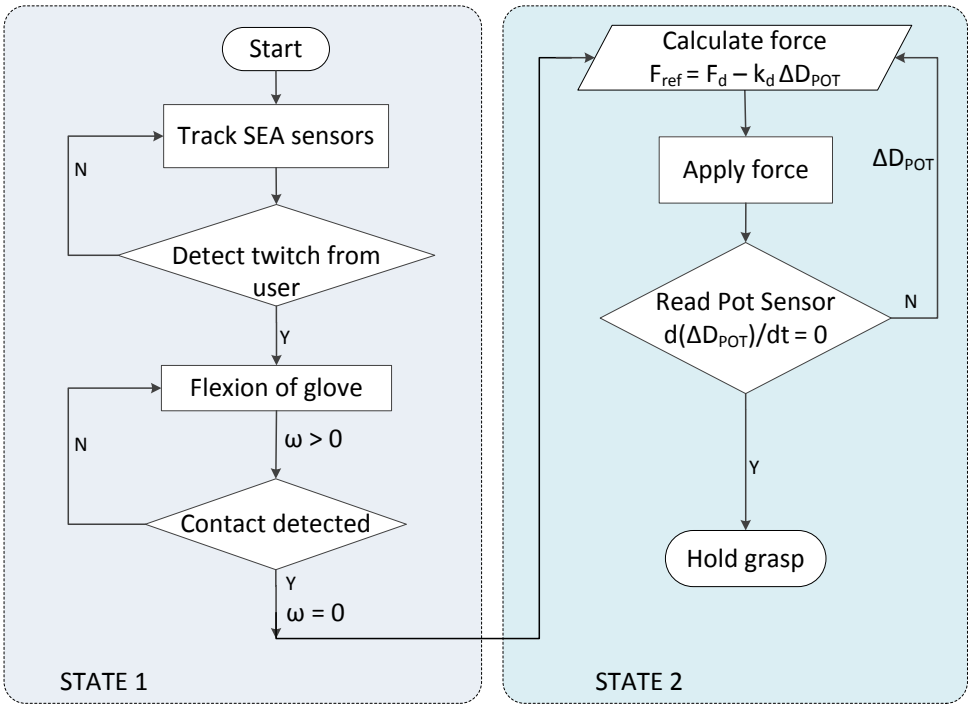

Figure 5.1: Flowchart describing the deformation detection algorithm

In the algorithm, ω is motor velocity, F_d is the initial predefined force provided to the algorithm, F_{ref} is the reduced force after detection of deformation, ΔD_{POT} is the deformation as measured by the linear potentiometer.

The magnetic hall encoder measures the motor position which could be used to measure the linear displacement of the end of the spring connected to the motor. As the glove applies force on the object, based on the deformation that is calculated based on the difference in sensor readings in the SEA, the force value is reduced online to minimize the deformation of the object. Figure 5.1 describes the deformation detection algorithm.

Before testing the algorithm on a physical prototype, a simulation was performed to test the algorithm. For the simulation, the object to be grasped was modeled as a linear spring based on results from the Finite Element Analysis (FEA) simulation performed on a shell type cylindrical object as shown in Figure 5.2 with transverse forces applied on the object.

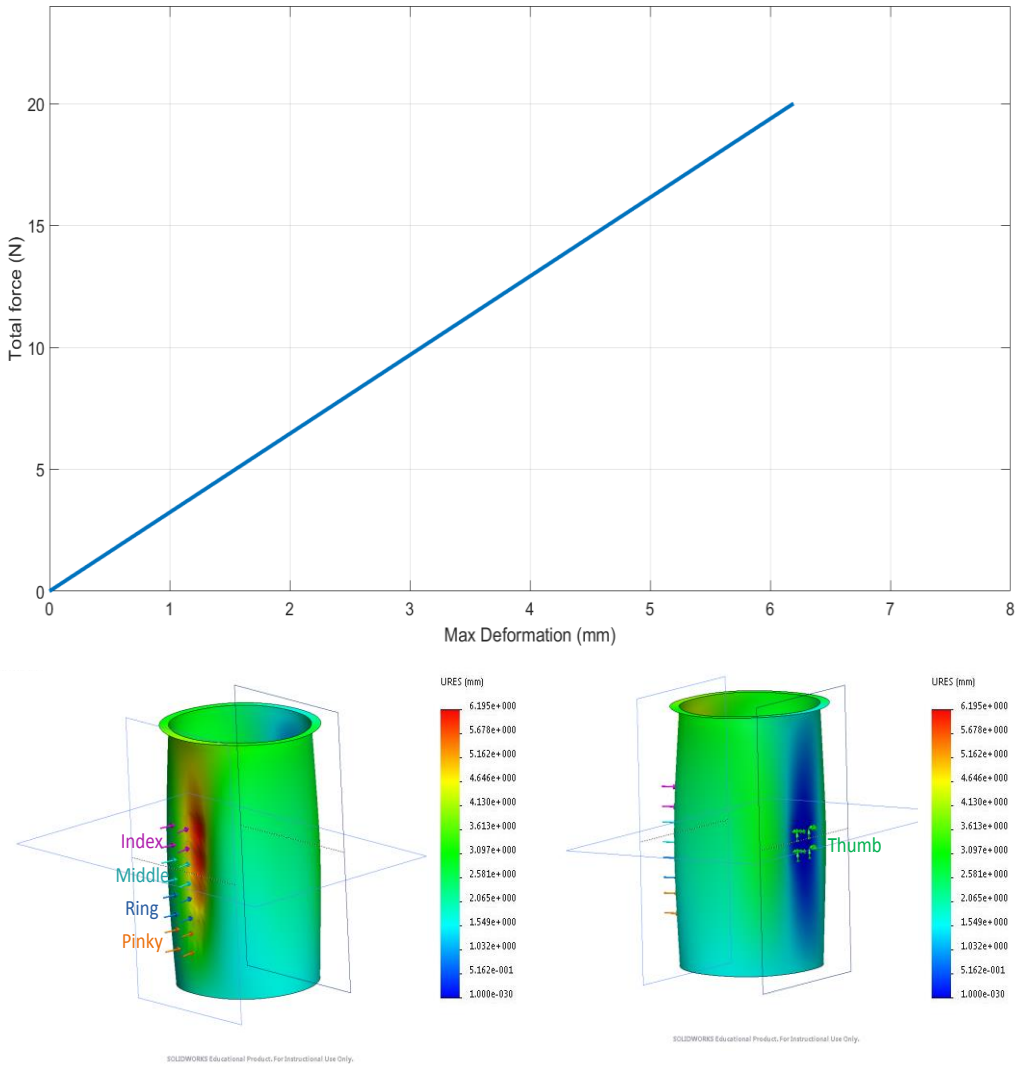

Figure 5.2: FEA analysis of thin film cylindrical object

The maximum displacement from the FEA simulation was found to be linearly dependent on the force being applied. The simulation was performed in SIMULINK and was tested on 4 different stiffness values of the object. Simple force control algorithm results are used for comparison with that of using the deformation detection algorithm.

In the simple force control, the force is applied in a manner such that it is equal to the predefined force irrespective of the deformation observed. And in the case of the deformation detection algorithm, the reference force is reduced in proportion to the deformation detected. Figure 5.3 clearly shows a difference between the deformation when a simple force algorithm is used compared to when a deformation detection algorithm is used. As can be noticed from the results, the deformation reduction is higher for softer objects as compared to stiffer objects. This implies that for rigid objects the algorithm will apply force that is more close to the initial predefined force.

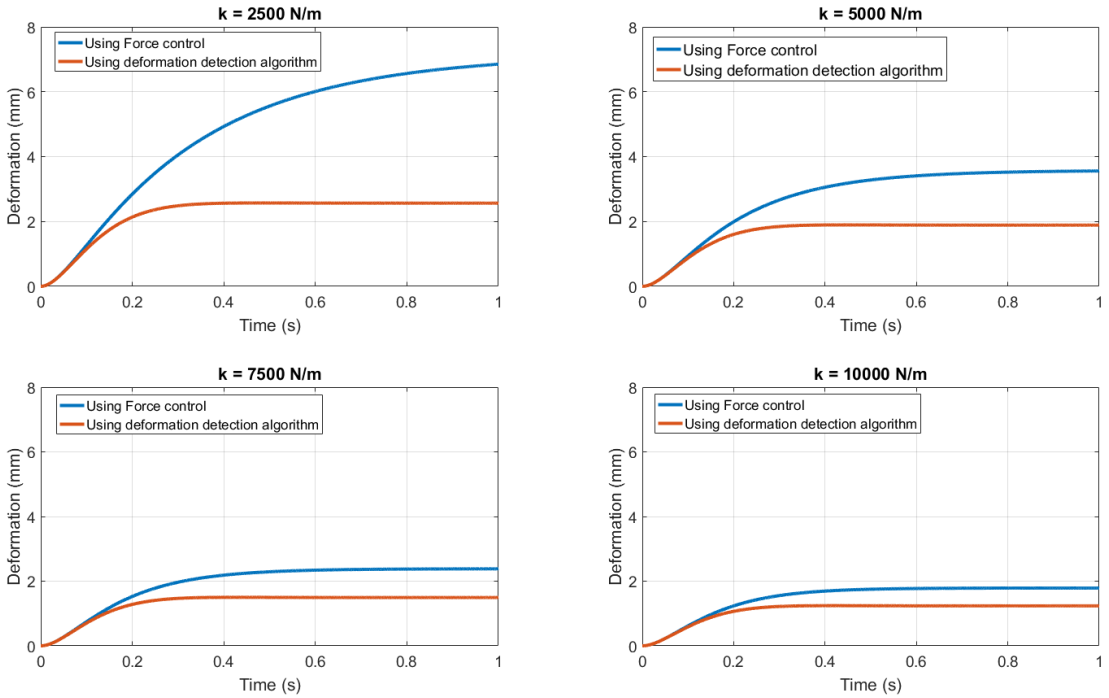

Figure 5.3: Comparison plot between using deformation detection algorithm and force control

5.2 Optimal Force Algorithm

As previously described, one of the conditions for a stable grasp is that the glove should apply forces such that the force and moment equilibriums are satisfied.

For the sake of simplicity, only cylindrical grasps were considered since they are the most common grasp type in daily life activities. Three points of contact are necessary and sufficient to grasp a 3D object, but while performing cylindrical grasp with the glove, five fingers come in contact with the object. Since there are more contact points than necessary, there will be infinite combinations of force distributions that can satisfy the force and moment equilibriums.

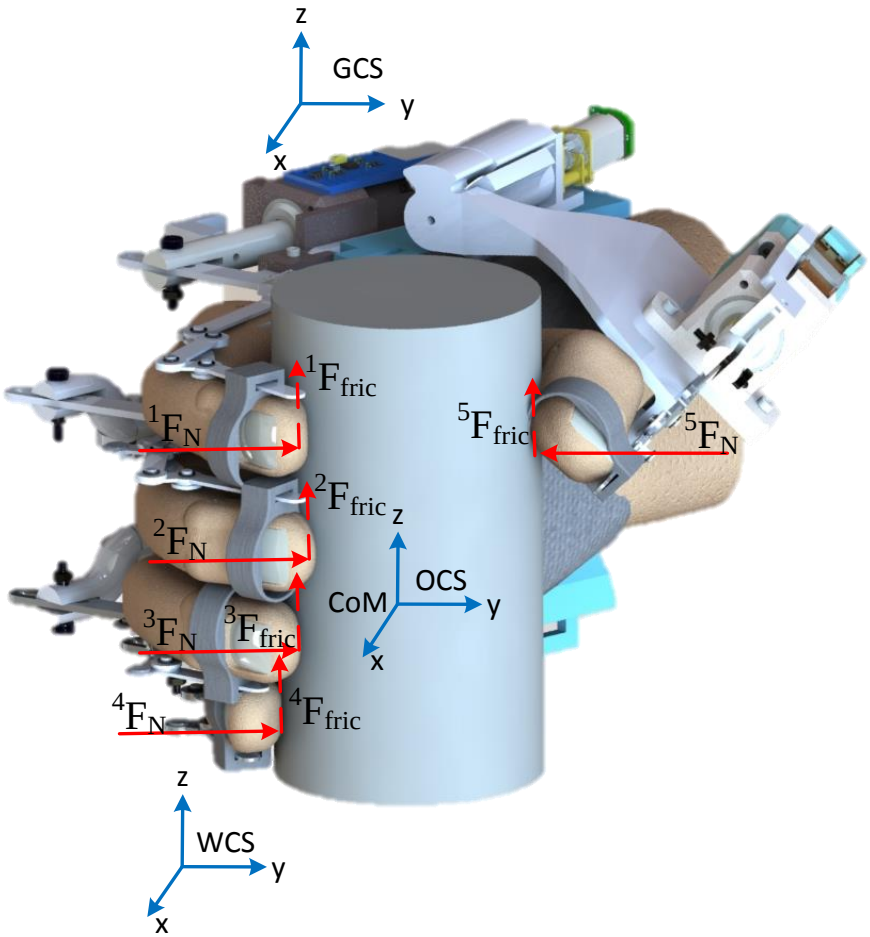

Figure 5.4: Forces on the object exerted by the glove

Therefore, an optimization method was used to find the optimal set of force distribution that meets the stability conditions. While grasping, the user may move the object in a translational or rotational motion or a combination of both. During this user imparted motion, the forces required to meet the equilibrium conditions also change in a dynamic manner. Therefore, an Inertial Measurement Unit (IMU) is used to measure the real-time kinematic state of the glove which is fed into the optimization algorithm to calculate the optimal set of forces.

5.2.1 Dynamic Modeling of the Grasp

The dynamics of grasping an object needs to be analyzed, which will be used in the optimization as constraint equations. Based on the Figure 5.4, showing simple cylindrical grasp, the contact forces are given according to Equation (5.1)

$$\sum_{k=1}^{5} \mathbf{S}_k \mathbf{F}_k + \mathbf{S}_{\mathbf{trans}} M\ddot{\mathbf{x}} + \mathbf{S}_{\mathbf{g}} M\mathbf{g} + \mathbf{S}_{\mathbf{rot}} I\ddot{\boldsymbol{\theta}} = 0 \qquad (5.1)$$

with

$$\mathbf{S}_k = \begin{bmatrix} R_{k\_cm} & p_{k\_cm} R_{k\_cm} \\ 0 & R_{k\_cm} \end{bmatrix}$$

$$\mathbf{F}_k = R_{w\_g} R_{g\_f} \begin{bmatrix} {}^{k}F_N \\ 0 \\ {}^{k}F_{fric} \end{bmatrix}$$

$$\mathbf{S}_{\mathbf{trans}} = \mathbf{S}_{\mathbf{rot}} = \begin{bmatrix} R_{imu\_cm} & p_{imu\_cm} R_{imu\_cm} \\ 0 & R_{imu\_cm} \end{bmatrix}$$

$$\ddot{\mathbf{x}} = \begin{bmatrix} a_x \\ a_y \\ a_z \end{bmatrix}, \ddot{\boldsymbol{\theta}} = \begin{bmatrix} \dot{\omega}_x \\ \dot{\omega}_y \\ \dot{\omega}_z \end{bmatrix}$$

where ${}^{k}F_N$ is the normal force applied by the k[th] finger on the object, ${}^{k}F_{fric}$ is the friction force due to the k[th] finger on the object, R_{k_cm} is the rotation matrix from the point of contact of k[th] finger to the center of mass of the object, p_{k_cm} is the translation matrix from the point of contact of k[th] finger to the center of mass of the object, R_{k_cm} is the rotation matrix from the IMU to the center of mass of the object, p_{k_cm} is the translation matrix from the IMU to the center of mass of the object. a_x, a_y and a_z is the linear acceleration along the three axes, ω_x, ω_y and ω_z are angular velocity of the object along the three axes and these parameters are calculated by the IMU placed on the glove. The above equations satisfy the equilibrium equations as required for meeting one of the stability conditions. Slip is prevented by making the forces satisfy Equation (5.2)

$$\sum_{k=1}^{5} \mu\, {}^{k}F_N \sin(\theta_z) \geq mg + m\ddot{x}_z \tag{5.2}$$

where μ is the friction coefficient of the object and θ_z is the orientation of the object with respect to the z-axis. The forces on the fingers ${}^{k}F_N$ are determined by performing optimization such that they meet the above given stability condition equations.

5.2.2 Optimization Method

For any optimization problem an objective function which will be minimized under given constraints needs to be formulated. For this case, two objective functions are proposed which are as given in Equation (5.3) and (5.4).

$$f(.) = {}^{1}F_N^2 + {}^{2}F_N^2 + {}^{3}F_N^2 + {}^{4}F_N^2 \tag{5.3}$$

$$f(.) = \max\left\{ {}^{1}F_N, {}^{2}F_N, {}^{3}F_N, {}^{4}F_N \right\} \tag{5.4}$$

Here we proceed with the objective function given by Equation (5.3) as solving the optimization problem using objective function given by Equation (5.4) is highly complex

and cannot be implemented on a microcontroller. This is a constrained optimization problem and in this case there is one equality constrained equation given by Equation (5.1) and one inequality constrained equation given by Equation (5.2). While performing optimization, there is a possibility for the optimal solution to be out of bounds, which cannot be implemented in real life. Therefore, the bounds on each design variable are given as in the Equation (5.5). The lower bound is chosen such that there are no negative values generated which can't be implemented as the linkage can only apply force in the push direction but not in pull direction. The upper bound is determined by the maximum actuator force limits

$$0 < \left\{ {}^{1}F_N, {}^{2}F_N, {}^{3}F_N, {}^{4}F_N \right\} \le F_{motorLim} \tag{5.5}$$

The optimization method used is a barrier method, which is an interior point method details of which are provided at [53]. This method requires a starting point which is feasible such that it satisfies the constraint equations. Therefore, an infeasible start newton method [53] is used simultaneously to find the feasible solution. This method allows any arbitrary point or set of force values as the starting point. The algorithm is detailed in Table 5.1.

Equation (5.6) is a simplified form of Equation (5.1) and the inequality Equation (5.2) comprises of box bounds on the design variables according to Equation (5.5) and the friction inequality equation as mentioned in Equation (5.2).

$$\begin{aligned} &\min \quad f_o = {}^{1}F_N^2 + {}^{2}F_N^2 + {}^{3}F_N^2 + {}^{4}F_N^2 \\ &\text{Subject to} \quad A[x] = b \\ &[x] = \begin{bmatrix} {}^{1}F_N & {}^{2}F_N & {}^{3}F_N & {}^{4}F_N \end{bmatrix}^T \\ &f_i \le 0, \qquad \text{i} = 1, 2, 3 \end{aligned} \tag{5.6}$$

where,

$$A = \begin{bmatrix} S_1 & S_2 & S_3 & S_4 \end{bmatrix}$$

$$b = -\left(\mathbf{S}_{\mathbf{trans}} M\ddot{\mathbf{x}} + \mathbf{S}_{\mathbf{g}} M\mathbf{g} + \mathbf{S}_{\mathbf{rot}} I\ddot{\boldsymbol{\theta}}\right)$$

$$f_1 = \begin{bmatrix} -{}^1F_N & -{}^2F_N & -{}^3F_N & -{}^4F_N \end{bmatrix}$$

$$f_2 = \begin{bmatrix} {}^1F_N - F_{motorLim} & {}^2F_N - F_{motorLim} & {}^3F_N - F_{motorLim} & {}^4F_N - F_{motorLim} \end{bmatrix}$$

$$f_3 = mg + m\ddot{x}_z - \sum_{k=1}^{5} \mu^k F_N \sin(\theta_z)$$

In the barrier method as mentioned earlier solves the problem of optimization problem with inequality constraints by transforming them to form a new objective function as shown in Equation (5.7) thus is converted to a problem with only equality constraints which can be solved using infeasible start newton method.

$$\begin{aligned} &\min \quad f_1 = t\left(f_0\right) + \phi\left(x\right) \\ &\text{Subject to} \quad A\left[x\right] = b \\ &\text{where,} \\ &\phi\left(x\right) = -\sum_{i=1}^{m} \log(-f_i(x)) \end{aligned} \tag{5.7}$$

where f_1 is the new objective function which includes the inequality constraint, t is a parameter which affects the accuracy. The optimal values are obtained in an iterative manner where the values are updated until they converge to the optimal value.

The force values of this optimization problem are converged to their optimal values in an iterative manner. Initially arbitrary values of force are chosen and using Equation (5.8), Δx is added to the initial force values in every iteration, until the value of force values converge to a particular value after several iterations.

Table 5.1: Optimal Force Algorithm

Input : choose arbitrary x such that, $x \in$ dom (f_0) and $f_i(x) < 0$ is satisfied

Input object properties such as mass, inertia etc.

Define parameters like Motor limits, distance between linkages

Read IMU data and fetch current acceleration and orientation of the object

Setup : Formulate new objective function f_1 as given in Equation (5.7)

Define the equality constraint equation matrices A and b

for i = 1 : 30

1. Find Δx using Equation (5.8)
2. Update $x = x + \Delta x$
3. Repeat step 1 with updated x value; Update i ++

end

Output : Optimal force values - x

The equation for updating the x value is described in Equation (5.8)

$$\begin{bmatrix} \Delta x \\ w \end{bmatrix} = \begin{bmatrix} \nabla^2 f & A^T \\ A & 0 \end{bmatrix}^{-1} \begin{bmatrix} -\nabla f \\ b - Ax \end{bmatrix} \tag{5.8}$$

The above algorithm was implemented in MATLAB and all the force values converged approximately in around 30 iterations as shown in Figure 5.5. The algorithm when implemented on teensy 3.6 microcontroller is executed in 12 ms by the end of 30 iterations.

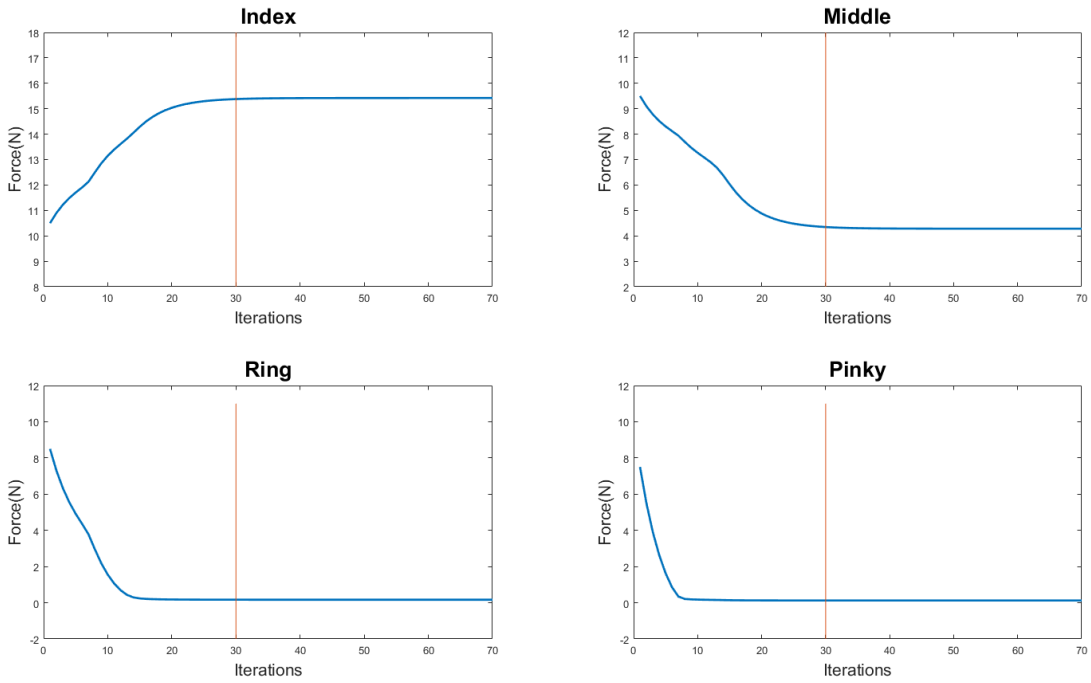

Figure 5.5: Force Convergence results of optimization

5.3 Controls Architecture

The force reference values for each actuator are generated by the optimization algorithm as described in the previous section. These target values are sent to a controller that drives the SEA towards the reference force value. To design the controller for the SEA, a transfer function of the SEA needs to be derived. Viscous friction was assumed to be present in the actuator. In the transfer function as given in Equation (5.9), the unknown parameters are the viscous friction coefficient and the Inertia which includes inertia of motor shaft, lead screw and linkage mechanism as observed by the motor. Estimation of these two parameters is achieved by using system identification technique. System identification requires input and output data either in the time-domain or the frequency domain based on which the transfer function of the plant is estimated that best matches with the output for the given input. The results of the estimated transfer function

as compared with experimental results for three different input cases are provided in Figure 5.6.

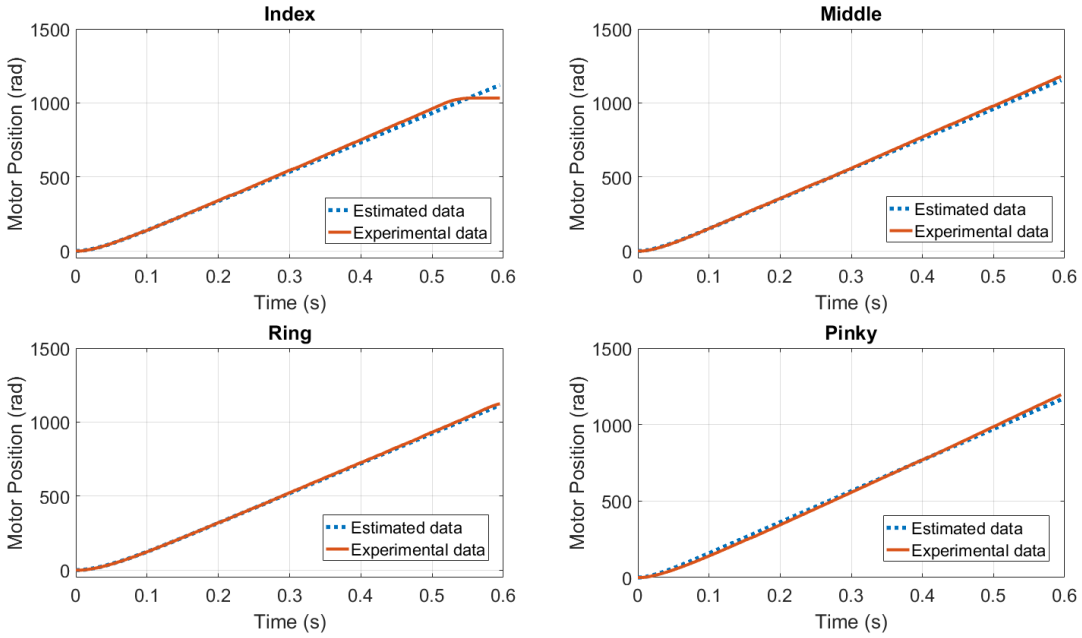

(a)

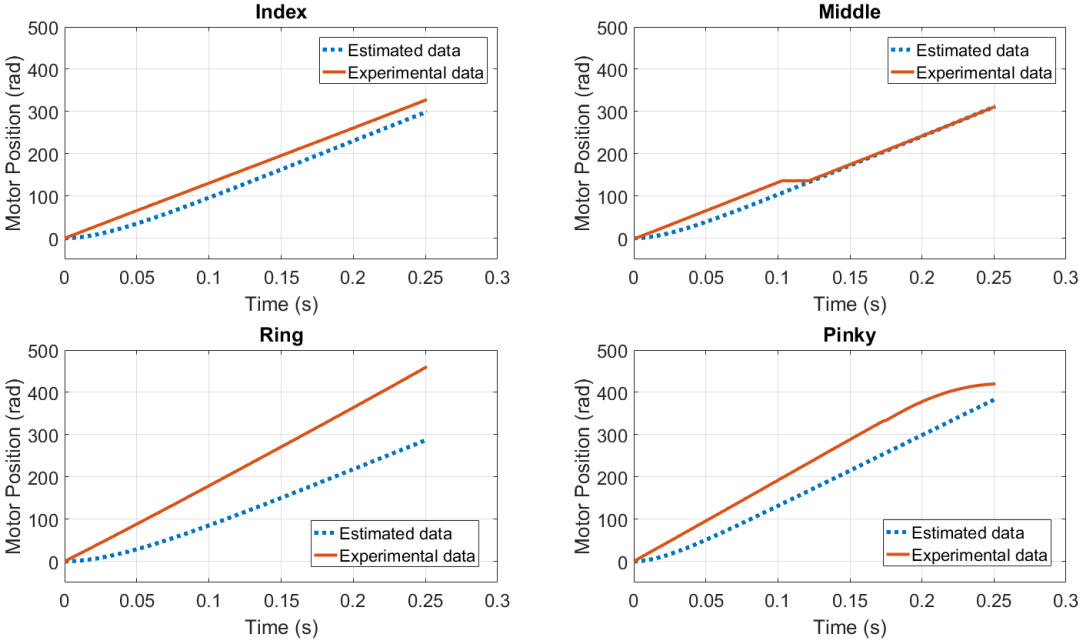

(b)

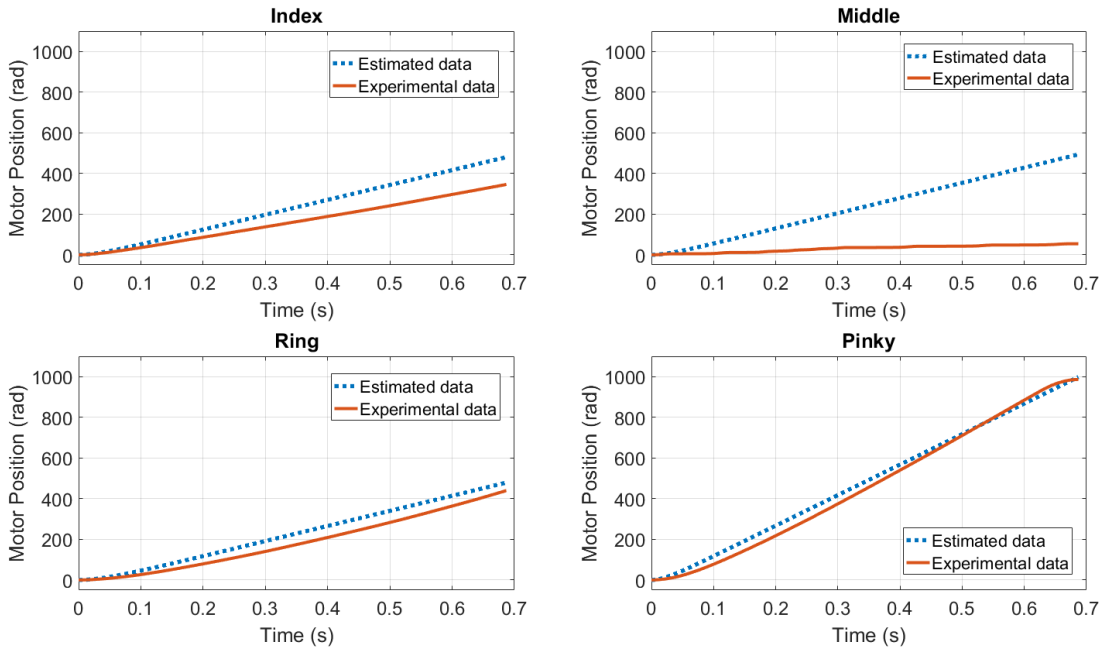

(c)

Figure 5.6: System identification results: (a) Input voltage 8.2 V (b) Input voltage 5.6 V (c) Input voltage 3 V

This data is acquired by sending a constant input voltage to the motor and measuring the linear position with respect time. This data is fed into the system identification application in MATLAB to estimate the transfer function.

$$\frac{\theta_m}{V} = \frac{k_t}{s^2 JR + s(bR + k_v k_t)} \tag{5.9}$$

Where, θ_m is the motor position (rad), R is motor resistance, k_t is torque constant of the motor, k_v is motor velocity constant, J is the effective inertia and b is effective viscous coefficient.

Motor controller is designed based on the estimated transfer functions. The output results of a tuned PID (Proportional-Integral-Derivative) and PI (Proportional- Integral)

controller in SIMULINK were similar so a PI controller is selected for the sake of simplicity of implementation. The PI controller gains are tuned in SIMULINK using PID tuner and the model was build using the transfer function which includes the dynamics of spring in linear SEA as given in Equation (5.10)

$$\frac{\theta_m}{V} = \frac{k_l}{s^2 JR / k_t + s(bR + k_v k_t) / k_t + Rk_s k_l^2 / k_t} \qquad (5.10)$$
$$k_l = \frac{P}{2\pi N}$$

Where, P is pitch of the leadscrew, N is gear ratio of gearhead of the motor and k_s is stiffness constant of the spring in SEA.

The transfer function is used to build the feedback physical model in SIMULINK is used to tune the PI gain parameters. The results of the tuned controller as briefly described in Table 5.2.

Table 5.2: Tuned controller results

	Index	**Middle**	**Ring**	**Pinky**
Bandwidth (Hz)	1.42	1.52	1.47	1.22
Rise time (s)	0.17	0.16	0.15	0.2
Settling time (s)	0.27	0.27	0.23	0.37
Overshoot (%)	0.74	0.23	1.74	0.02

The force measured by the SEA is non-linearly related to the force that is being applied at the tip of the finger where the object is being grasped. Therefore, a Jacobian transformation was applied to relate the force exerted by the SEA and force applied at the fingertip.

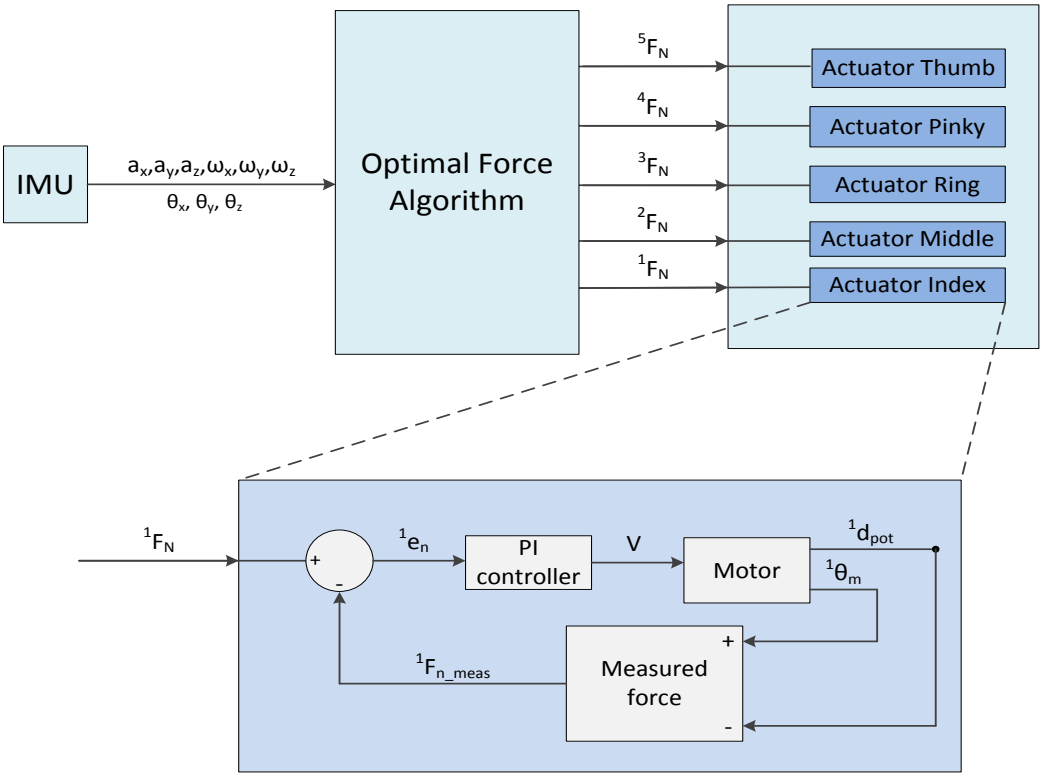

Figure 5.7: Overall control architecture of the glove

Equation (5.11) describes the relation between the input and output of the controller and the relation between the force measured by SEA and fingertip force.

$$\begin{aligned} e_i &= {}^iF_d - {}^iF_m \qquad i = 1,2,3,4 \\ {}^iF_d &= J_i\,{}^iF_N \\ {}^iF_m &= k_{spr}({}^id_{pot} - c\,{}^i\theta_m) \\ V &= {}^ik_p e_i + {}^ik_{\text{int}}\int e_i dt \end{aligned} \tag{5.11}$$

where ${}^iF_m$ is the measured force by the SEA, ${}^iF_d$ is the desired reference force by the SEA, k_{spr} is the SEA spring constant, ${}^id_{pot}$ is the linear potentiometer measurement and ${}^i\theta_m$ is the motor position measured by the magnetic hall-effect encoder.

The Jacobian (J) for each finger is derived using the dynamics model developed in [54]. As can be seen, the dynamics model is highly non-linear and a direct

implementation on micro-controller will pose computation issues. An approximate 2nd order polynomial model was fitted to the analytical dynamics model as shown in Figure 5.8 and will be used in the Jacobian.

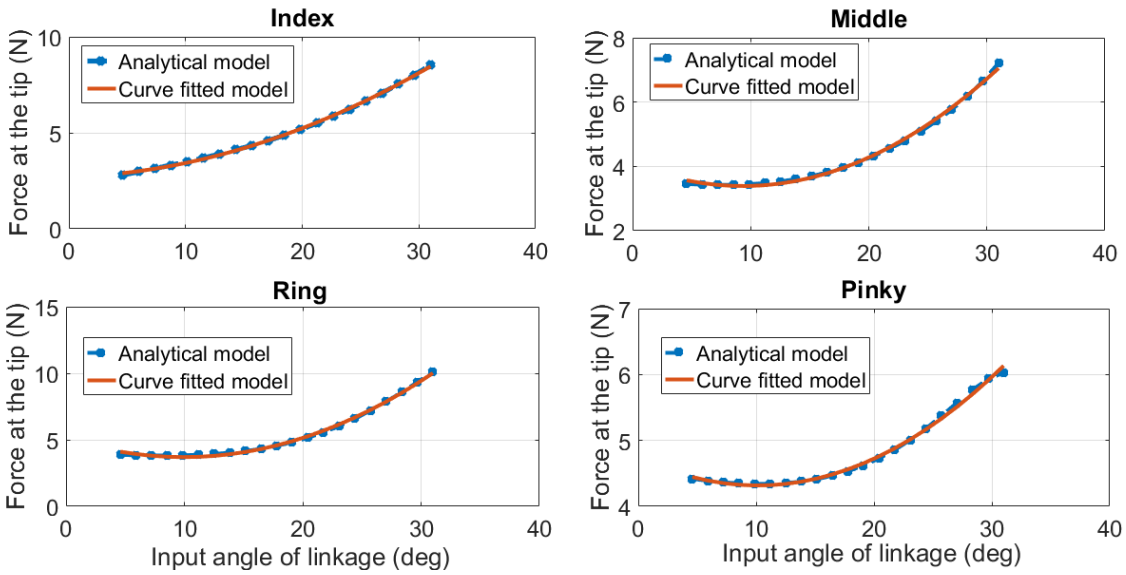

Figure 5.8: Fitted force model for each finger

5.4 Conclusion

Based on simulations performed in MATLAB, it was observed that the deformation detection algorithm was simple enough to be implemented on a microcontroller with limited computation resources, but also prevent the object from further deformation. The reduction in deformation is higher for low stiffness objects and vice versa. These simulations were performed under the condition that the object behaves as a linear spring with constant stiffness. Analytical derivations for the optimal force algorithm were described. The algorithm was implemented in MATLAB and was able to converge to the optimal values in 30 iterations which show that this algorithm can be run

on a microcontroller without introducing large delay into the system when operating in real-time.

CHAPTER 6

EXPERIMENTAL SETUP AND RESULTS

The RML glove was designed in SolidWorks and manufactured and integrated to test both algorithms described earlier. The glove base structure and most of the SEA parts including the screw-nut were manufactured using 3D printer. The linkages were manufactured from a 0.8 mm thick Aluminum sheet using a 2.5D milling machine so that it is sufficiently strong and lightweight. DC brushed motors were used with 250:1 gearbox and runs on 12 V power supply with stall torque of 0.3 N-m. For measuring the motor position, magnetic hall-effect encoders were used which provide 12 counts per revolution of motor shaft. The output of the SEA was measured by using a linear potentiometer with 20 mm travel length. The actuators were controlled using teensy 3.6 microcontroller which also runs the deformation detection algorithm and optimal force algorithm. The micro-controller sends the motor PWM (Pulse Width Modulation) signals to the motor driver (by TI DRV8801) which can deliver a continuous current of 1 A and can operate between 8V and 36V. MPU-9250 by InvenSense IMU was used for measuring the orientation and acceleration of the glove. It is a 9-axis motion tracking device that combines a 3-axis magnetometer, 3-axis accelerometer, and 3-axis gyrometer. Magnetometer provides orientation of the device with respect to the magnetic north, the Accelerometer provides the gravity and linear acceleration measurements along the three axes, and the Gyrometer provides angular velocity about the three axes. Figure 6.1 presents the prototype while being worn on a human hand.

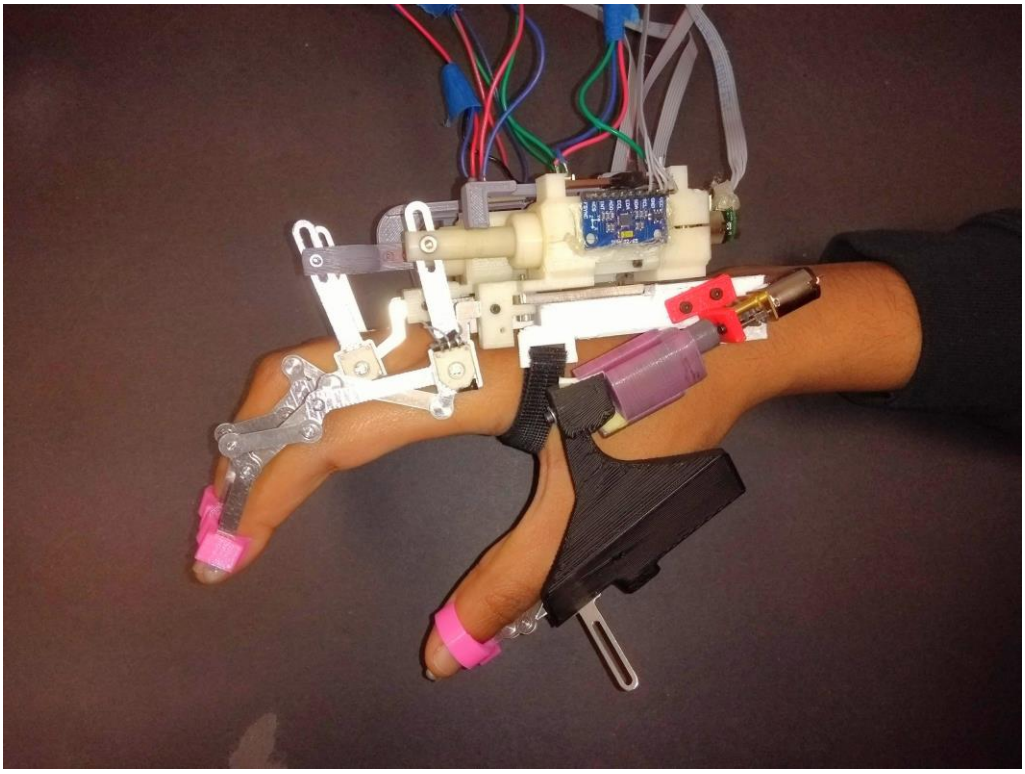

Figure 6.1: RML glove prototype

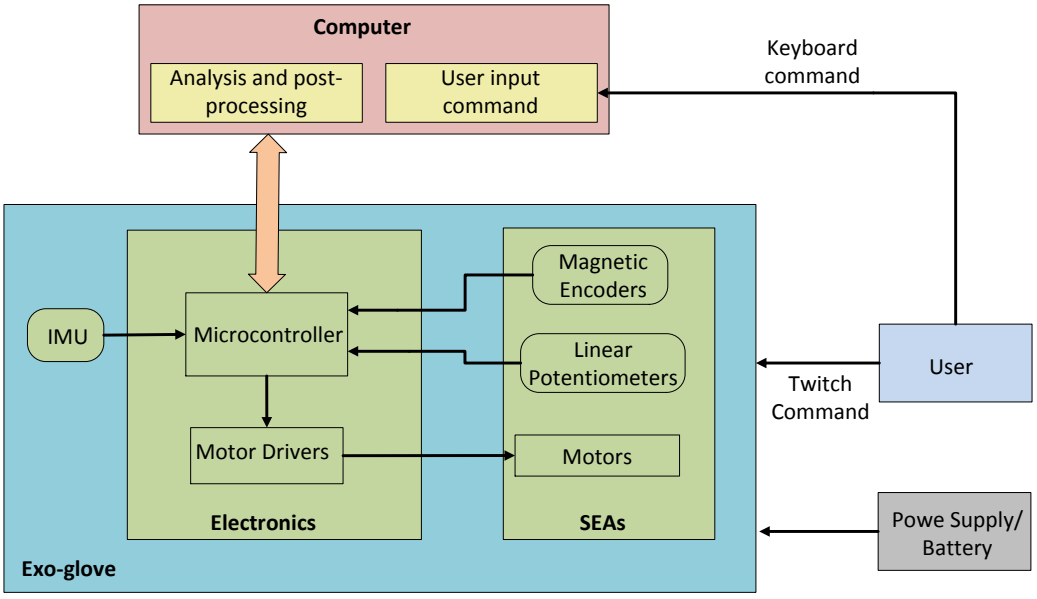

Figure 6.2: Overall hardware architecture

Exponential filter was used to remove noise from all the sensors including the IMU, linear potentiometer and magnetic hall-effect encoders.

6.1 Experimental Results

6.1.1 Deformation Detection

In this test, a deformation detection algorithm was implemented and tested on the glove. Three different objects were selected with different stiffness for the test including a plastic water bottle, a polycoated paper cup, and a plastic cup.

Initial tests were carried out on these three objects to quantitatively measure the stiffness of the objects. The test setup as shown in Figure 6.3 includes a linear actuator with a Force Sensitive Resistor (FSR) at its tip. The linear servo actuator was placed against the surface of the object such that it was slightly touching.

Then the linear actuator was commanded to move forward such that it pushes against the object while deforming it. The FSR was used to calculate the force applied by the linear actuator on the object and the potentiometer was used to calculate the distance travelled by the linear actuator which represents the deformation of the object. This test was carried out for all three objects and results of the tests are depicted in Figure 6.4. The measured data is fitted to a linear curve and is plotted along with it for comparison. By observation, it is clear that the plastic water bottle is stiffer than the poly coated paper cup which is also stiffer than the plastic cup. Since the stiffness properties of the objects were obtained, the next tests with the glove were performed.

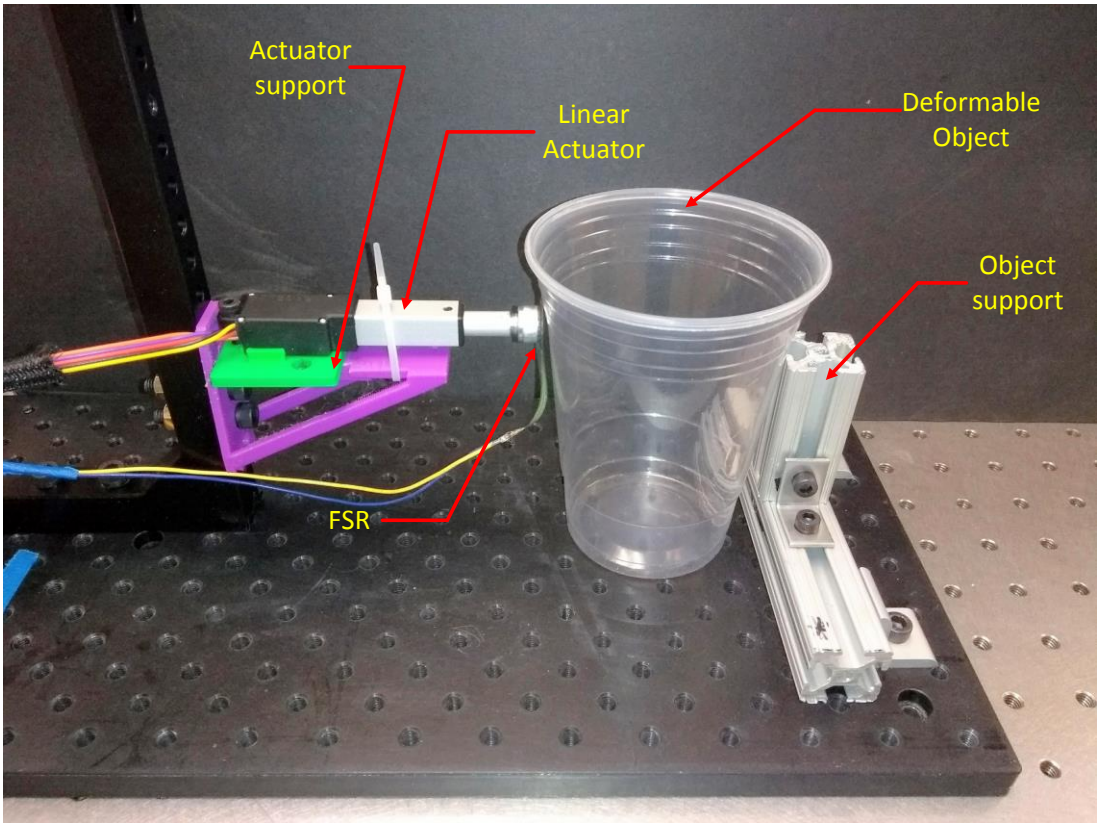

Figure 6.3: Material stiffness testing setup

The deformation detection algorithm was implemented and the deformation is measured. Initially the glove was positioned near the object to be grasped and all the linkages were fully extended so they are not touching the object. Then constant velocity input was applied in a feedforward manner, such that the fingers start flexion and closing on the object. As soon as the finger makes contact with the object, the contact is detected based on the acceleration spike observed in the linear potentiometer measurements as shown in Figure 6.5. The particular linkage upon making contact with the object halts the flexion and waits until all the fingers achieve contact. After all the fingers make contact, the deformation detection algorithm is engaged and the glove starts grasping the object with predefined force. While performing this grasp, the linear potentiometer and magnetic encoder readings are measured and stored for analysis. This test is repeated for

all the three objects and all the measurements are stored. This test is repeated for all three objects with only the force control implemented results that were used for comparison with the former test results.

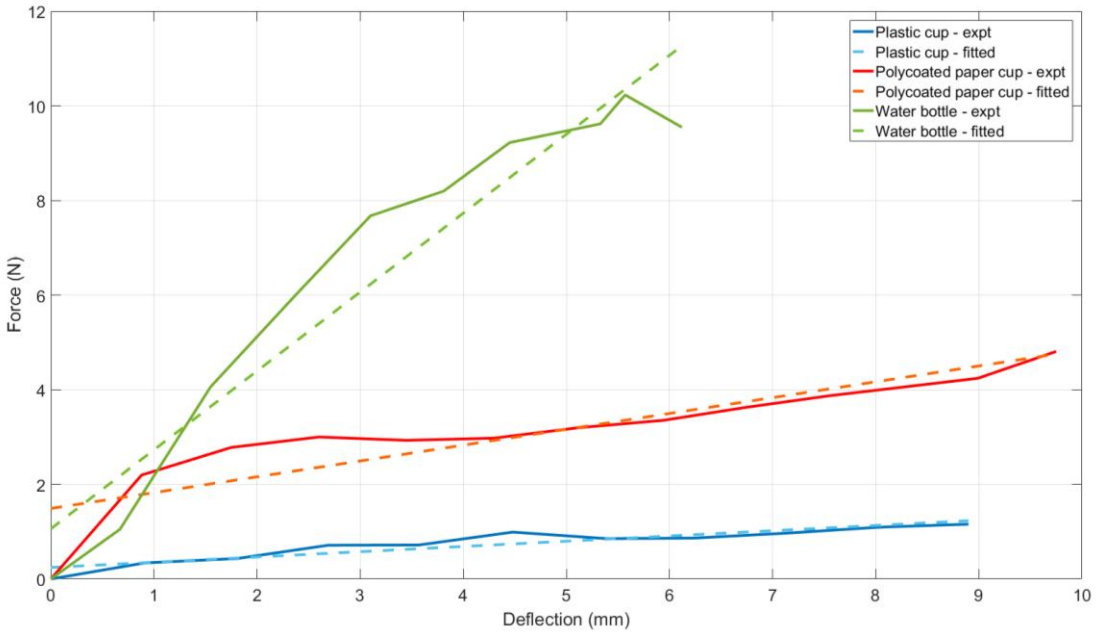

Figure 6.4: Measured stiffness plot

As can be seen in the Figure 6.6, the plots are arranged in increasing stiffness of the object and the gap between the deformation for force control and deformation detection algorithm is decreasing with increasing stiffness as observed in the simulation results. This proves that the algorithm decreases the force applied proportional to the softness of the object.

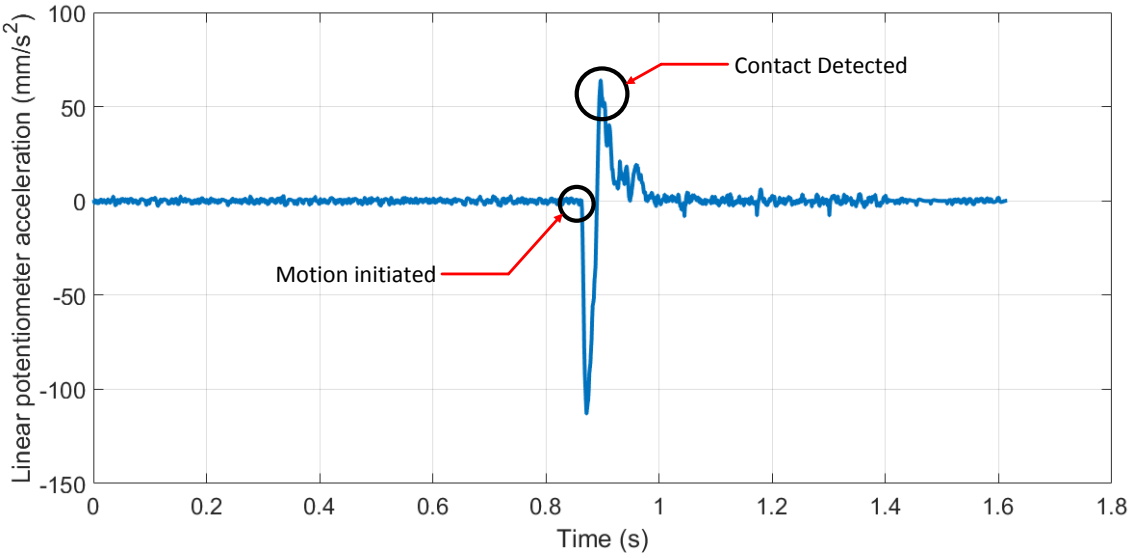

Figure 6.5: Contact detection during grasping

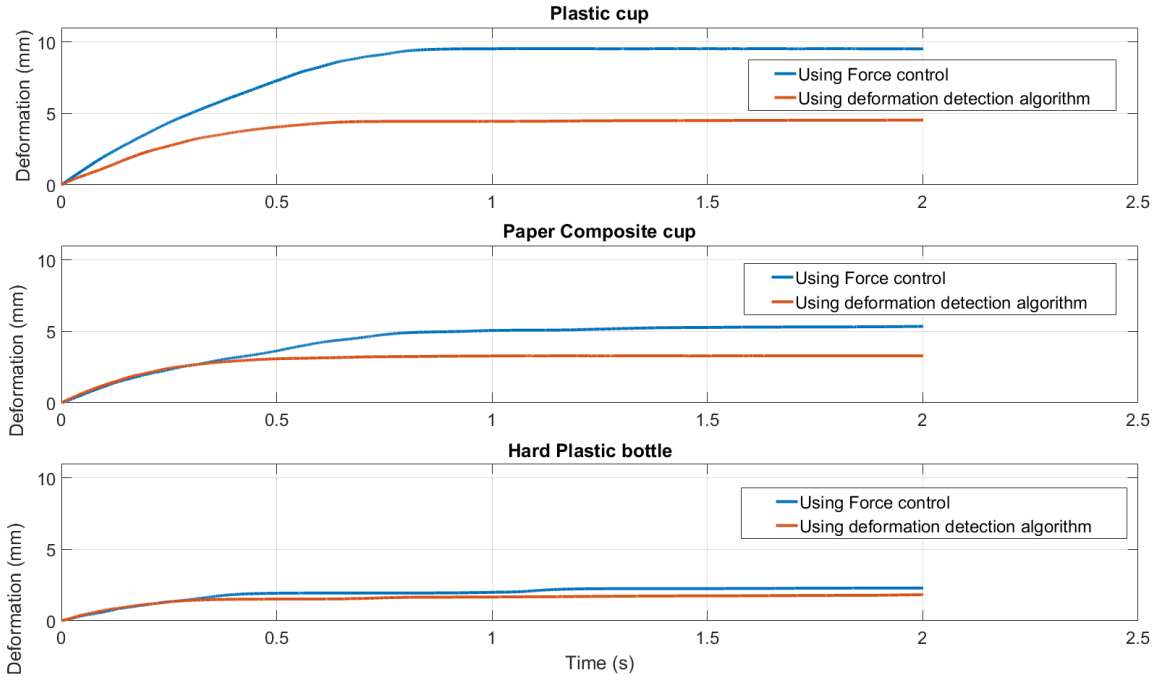

Figure 6.6: Measured deformation algorithm response

6.1.2 Optimal Force Algorithm

A test where the forces from the optimization are compared with forces produced by a human hand were performed. The test setup includes an object (water bottle) and four FSR sensors are attached on the bottle surface at known relative distances as shown in Figure 6.7. An IMU is attached on the object at known distance from the region of grasp. Then the bottle is held by a healthy hand such that the four fingers are on top of the four FSR sensors.

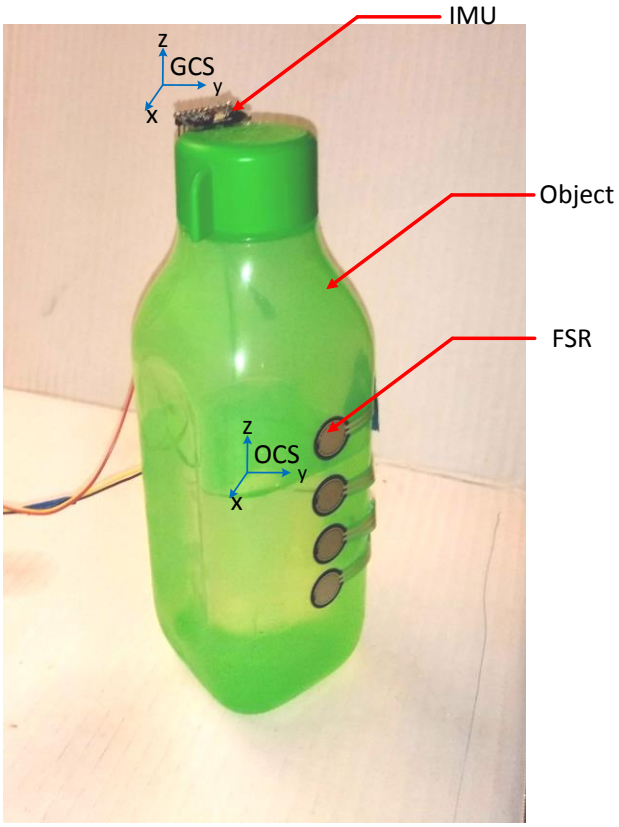

Figure 6.7: Hand optimal test setup

Three sets of experiments were performed:(1) Hold the bottle in the air without any movement; (2) Hold the bottle up and then translate in the direction of the force applied by the fingers back and forth 3-4 times; and (3) Hold the bottle up and rotate the bottle in

both clockwise and counter-clockwise direction. While performing these tests, inertial data from the IMU and force data from the FSR are stored for post-processing. Hardware-in-Loop (HIL) simulation were performed where the data from the IMU was passed through the optimal force algorithm to generate the force distribution across the four fingers. Upon comparing the experimental data and the HIL simulation data as shown in Figure 6.8, it can be observed that for all three cases the middle and ring finger forces match with greater accuracy. However, the pinky finger force had less matching pattern in terms of force magnitude. This test was done to check the ability of the algorithm in producing human like forces. It can be concluded that two out of the four fingers exhibited acceptable matching in force magnitudes. The index finger matches partially with the experimental data and pinky finger demonstrates the lowest matching.

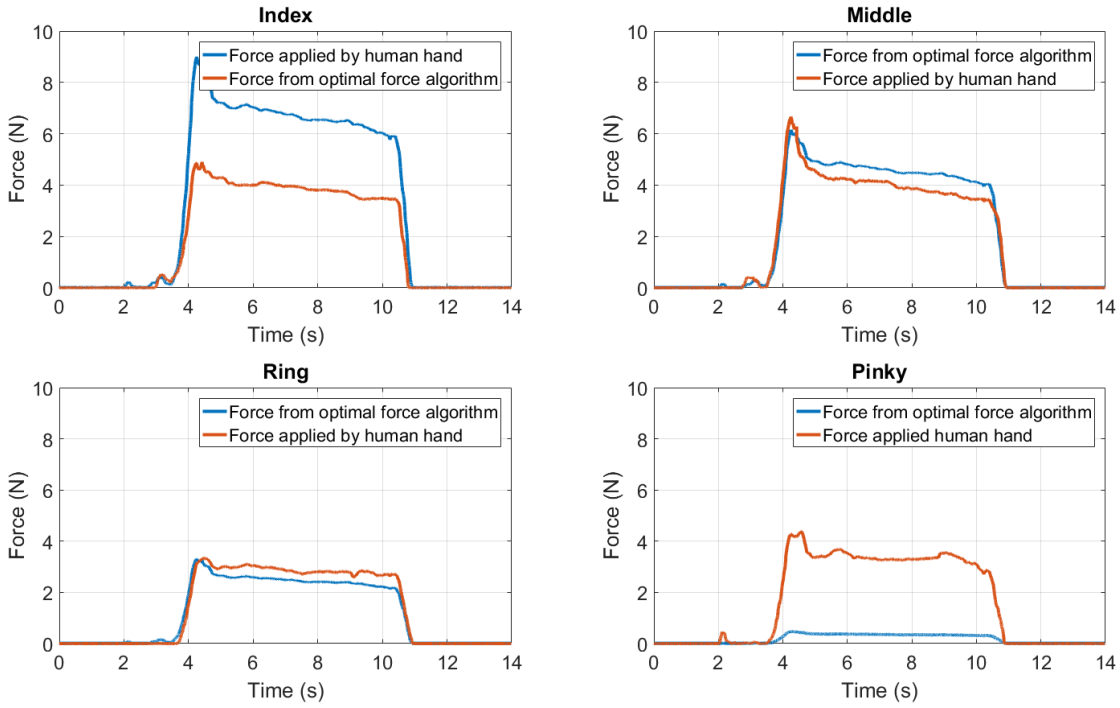

Figure 6.8: Hand optimal test for object holding

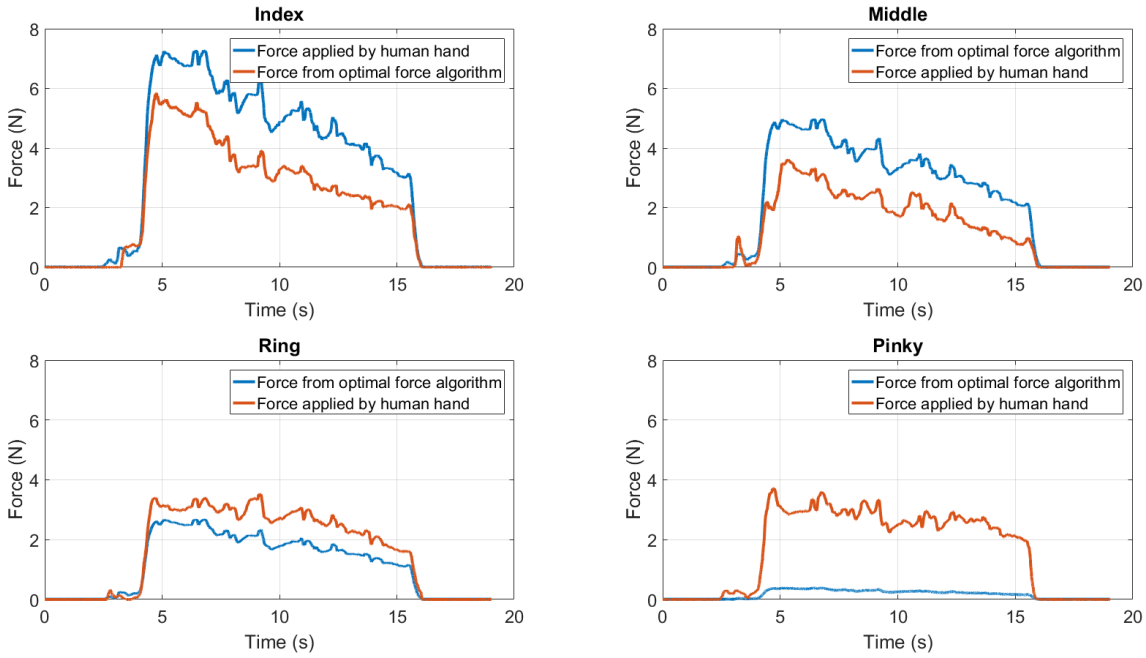

Figure 6.9: Hand optimal test for object translation

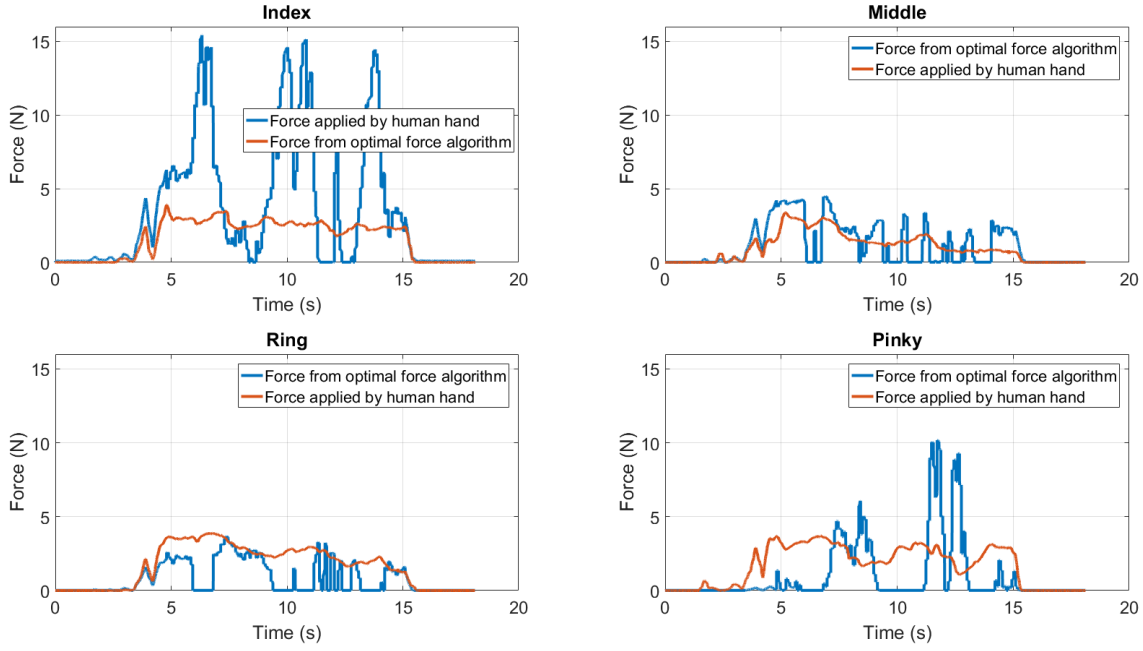

Figure 6.10: Hand optimal test for object rotation

The algorithm was then implemented on the RML glove for testing. Two tests were

Figure 6.11: Experiment setup for glove prototype testing

performed: (1) Predefined grasp force was applied and the object was held stationary, and (2) Initially the object is lifted after applying a predefined grasp after which it is slowly rotated 90^{o} clockwise and then back to the original position. The forces for each finger were determined by the optimization algorithm and the inertial data from the IMU.

From Figure 6.12, it can be observed that all the fingers of the glove reach the desired force with a small steady state error. The rise time is approximately 1.5 sec which is due to motor and power limitations.

In the object rotation part of the test as shown in Figure 6.13, the desired force is changing as it is rotated and the SEAs have approximately followed the force profile. There was small delay between changes occurring in the desired force and the measured force which is due to motor velocity and power limitations as mentioned earlier.

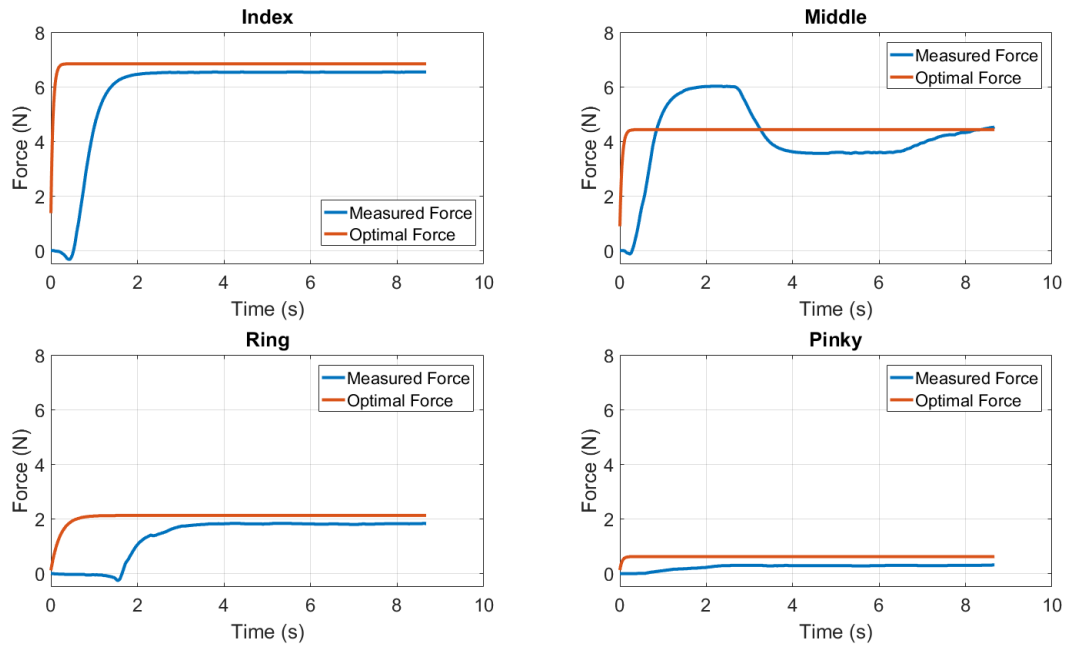

Figure 6.12: Test results for holding on the object with the glove

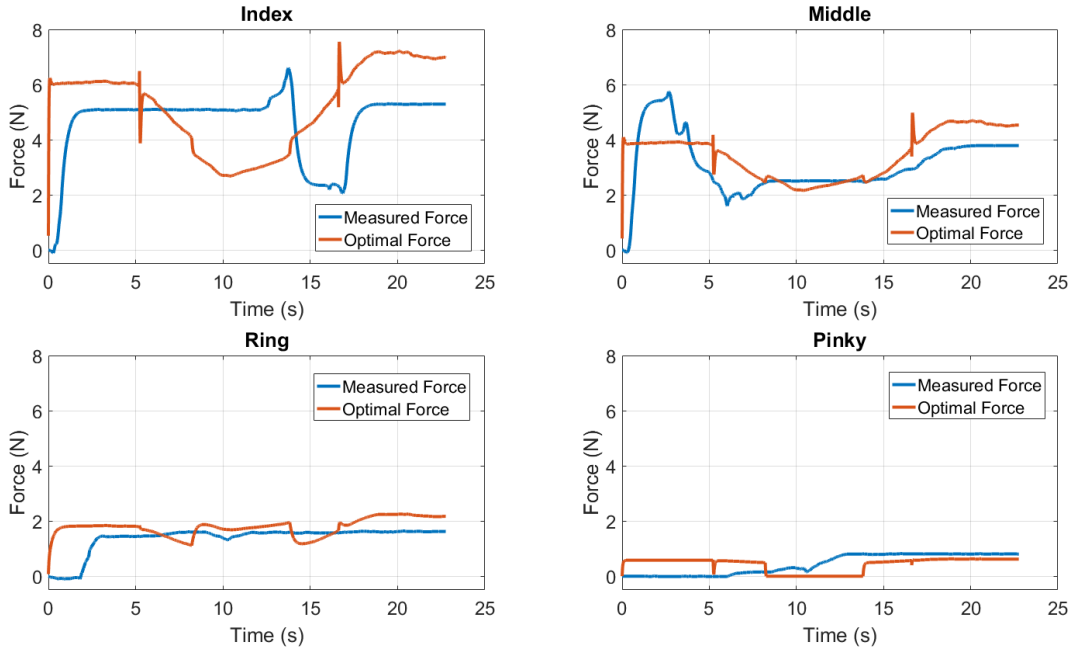

Figure 6.13: Test results for rotation of the object with the glove

6.2 Discussion

For deformation detection test, three objects with different stiffness were selected and initial tests were performed to calculate their approximate stiffness. Then, the RML glove was made to grasp these three objects while the algorithm was running. Then, simple force control was applied where it did not detect deformation. The two test results were compared and there was a clear difference in the deformation caused.

For optimal force test, the algorithm takes 12 ms to converge to the optimal force values thus this delay has very insignificant effect on the response of the system. Upon comparing with the forces applied by the hand and the force produced by optimization process, it can be said that for the ring and middle fingers the forces are very similar. But the forces for the index and pinky fingers showed a discrepancy, with the pinky finger with the largest discrepancy. This test shows that even though the optimization process doesn't exactly replicate the human hand force distribution, it does so partially with good overall pattern. With the use of faster and more powerful actuators, this algorithm could improve the grasp stability to a greater extent.

CHAPTER 7

CONCLUSION AND FUTURE WORK

This chapter concludes the thesis with a summary of the current work as well as the potential work in the near future.

7.1 Summary

In this research, novel algorithms were developed which improve the grasp stability of an exoskeleton glove by using minimal sensors and low computational power. The algorithms helped improve the stability of grasp in two major ways: (1) By detecting any deformation in the object while grasping and minimizing it, and (2) By adjusting the force distribution among the fingers such that the force and moment equilibriums are maintained. Deformation is detected based upon tracking of the potentiometer and encoder readings and then decreasing the set point force value to prevent further deformation. The force optimal algorithm developed used information from the sensors and the IMU to calculate an optimal distribution of forces that satisfy the force and moment equilibriums. The Barrier method along with the infeasible start newton method was used for optimization and was implemented in a teensy microcontroller. It took 11 milliseconds to run the optimization algorithm and was fast enough to have negligible errors. A full prototype was manufactured and integrated using 3D printed and machined parts and was used to test and validate the proposed algorithms. The deformation detection algorithms implemented on the prototype produced similar results compared with the simulation. The glove was able to differentiate between objects with different

stiffness and was able to reduce the deformation compared to when the algorithm was not implemented. The deformation reduction was higher for soft objects compared to rigid objects. Then the optimal grasp algorithm was implemented which, for known mass properties of the object, calculates the optimal forces for the four fingers. The thumb finger acted as a rigid support and provided a reaction force. Initial test comparing the simulation results with a human hand shows matching on two fingers and close similarity for the other two fingers. The glove performance was then tested for this algorithm.

7.2 Future Research

Future research includes combining both algorithms so that they run simultaneously. Integration of rotary SEA or some other form of sensor for autonomous estimation of the mass of the object and other properties will be performed. Improvements in mechanical design of the glove will be performed such that it is lighter and more compact. Machine learning techniques can be applied to improve the performance of these algorithms.

Further research can be performed by analyzing the computational cost, complexity, accuracy of the non-linear constrained optimization method, results of which can be used to further improve the optimization method. In depth study of friction characteristics needs to be studied to eliminate the delay issue and also experiment with different sliding materials in the linear actuator so as to have a uniform friction characteristics that is not affected by the load, velocity or position of the SEA.

7.2.1 Adaptive Grasp

The proposed algorithm uses the RSEA described in earlier chapter, at the thumb joint to estimate the mass of the object being grasped. The glove, after detecting the intention to grasp from the user, will start applying forces on the actuator to reach soft limits until no deformation is detected. After that, as the user is lifting the object, based upon the orientation measured from the IMU and torque sensed by the RSEA, the glove will apply additional gripping force on the object while satisfying the stability conditions. ADAMS simulation was setup to show that there will be a moment induced at the thumb joint when the glove is grasping an object.

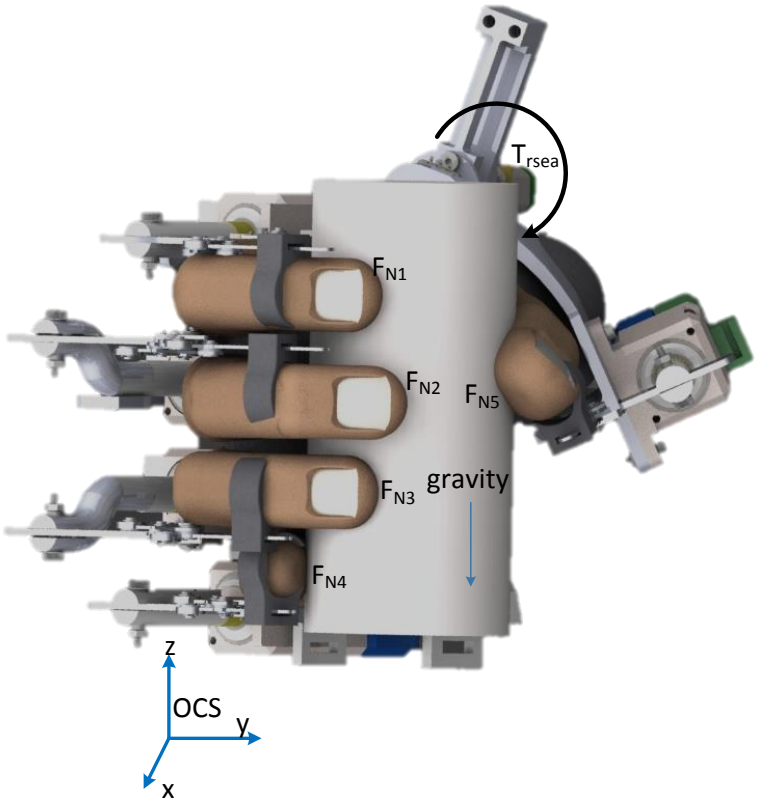

Figure 7.1: Forces on an object held by the hand assisted by the glove

After the forces reach soft limits, the object is lifted up when the RSEA starts sensing a force moment/torque on its axis. The gripping forces are increased in proportion to the rate at which the force moment is increasing. When the moment stops increasing, the gripping force is no longer increased. The forces applied on the fingers are optimal forces which satisfy the stability conditions for grasping. Figure 7.2 explains the algorithm for the above process.

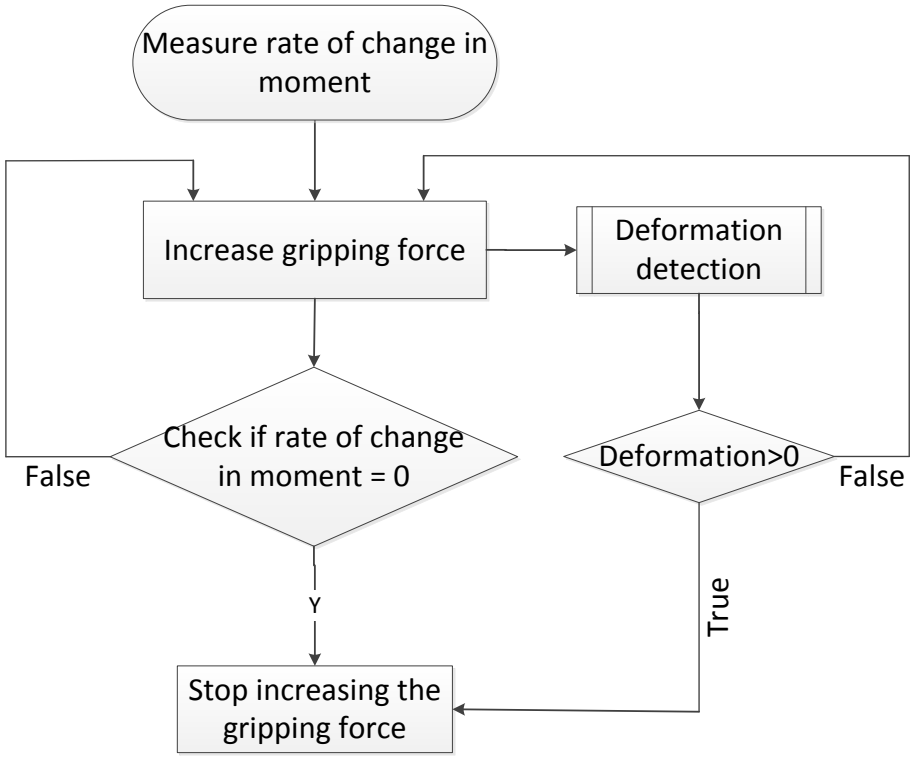

Figure 7.2: Algorithm flowchart describing the adaptive grasp with the deformation detection algorithm

The friction coefficient is calculated based on force applied at the thumb linkage and the moment measured at the RSEA as shown in Equation (7.1).

$$T_{rsea} = R_{IMU} d(\theta_{rsea}) F_T \qquad (7.1)$$

$$F_g = F_{\text{int}itial} + kT_{rsea} \qquad \text{if no deformation detected}$$

$$F_g = F_{\text{int}itial} + k_1 T_{rsea} - k_2 \dot{d}_{pot} \qquad \text{if deformation detected}$$

Where, T_{rsea} is the moment measured by the RSEA, R_{IMU} is the perpendicular distance between RSEA shaft and thumb point of contact, θ_{rsea} is the deflection of RSEA, F_T is the force measured by thumb, $F_{initial}$ is the initial soft gripping force, F_g is the new gripping force as calculated based on the mass of the object. Machine learning techniques can be used to improve the estimation process thus reducing the chances of the grasped object from slipping.

NOMENCLATURE

l_1, l_2 & l_3	Link length
c_1, c_2	Constraint link length
θ_1, θ_2 & θ_3	Joint angles of links
φ_1, φ_2, φ_3, φ_4	Angles of constraint joints with respect to the global y-axis
d_1, d_2, d_3 & d_4	Distance between constraint joint and link joint
w_1, w_2	Weighting parameters in linkage optimization objective function
e_1, e_2	Absolute errors of θ_2 and θ_3 respectively
x_k, y_k	Tip coordinates of link l_3 calculated from θ_1, θ_2 and θ_3
x_h , y_h	Tip coordinates of link l_3 calculated from joint angles obtained from a specific grasp in the HUST dataset
F_r	Normal force on flexible element of RSEA
m_r	Mass of the weight producing the torque on RSEA
θ_b	Angle made by the flexible element of RSEA
θ_r	Deflection angle of the RSEA shaft
θ_0	Initial angle of the shaft
l_m	Distance at which object is from the axis of shaft
E	Modulus of elasticity of the elastic beam
I	Moment of inertia of the beam
r	Distance between axis of shaft and center of pin applying force on the beam
l	Length of elastic beam
δ	Horizontal distance displaced by the pin
ω	Motor velocity
F_d	Initial predefined force provided to the Deformation detection algorithm
F_{ref}	Reduced force after detection of deformation
ΔD_{POT}	Deformation as measured by the linear potentiometer
${}^{k}F_N$	Normal force applied by the k^{th} finger on the object

${}^{k}F_{fric}$	Friction force due to the kth finger on the object
R_{k_cm}	Rotation matrix from the point of contact of kth finger to the center of mass of the object
p_{k_cm}	Translation matrix from the point of contact of kth finger to the center of mass of the object
R_{imu_cm}	Rotation matrix from the IMU to the center of mass of the object
p_{imu_cm}	Translation matrix from the IMU to the center of mass of the object
a_x, a_y and a_z	Linear acceleration along the three axes
ω_x, ω_y and ω_z	Angular velocity of the object along the three axes
μ	Friction coefficient of the object
θ_z	Orientation of the object with respect to the z-axis
f_1	New objective function which includes the inequality constraint
t	Parameter which affects the accuracy
θ_m	Motor position (rad)
R	Motor resistance
k_t	Torque constant of the motor
k_v	Motor velocity constant
J	Effective inertia
b	Effective viscous coefficient
${}^{i}F_m$	Measured force by the SEA
${}^{i}F_d$	Desired reference force by the SEA
k_{spr}	SEA spring constant
${}^{i}d_{pot}$	Linear potentiometer measurement
${}^{i}\theta_m$	Motor position measured by the magnetic hall-effect encoder
k_s	Stiffness constant of SEA spring
P	Pitch of leadscrew
N	Gear ratio of motor gearhead

ABBREVIATIONS

SEA	Series Elastic Actuator
FSR	Force Sensitive Resistor
DoF	Degrees Of Freedom
IMU	Inertial Measurement Unit
RSEA	Rotary Series Elastic Actuator
OCS	Object Coordinate System
WCS	World Coordinate System
GCS	Glove Coordinate System
ADL	Activities of Daily Life
RRR	Revolute- Revolute-Revolute
RoM	Range of Motion
RML	Robotics and Mechatronics Lab
SAFER	Sensing and Force feedback Exoskeleton Robotic Glove
HUST	Huazhong University of Science and Technology
CAD	Computer Aided Design
FEA	Finite Element Analysis
PID	Proportional Integral Derivative
PI	Proportional Integral
PWM	Pulse Width Modulation
HIL	Hardware in Loop

REFERENCES

[1] Kiger, P. J., "How GE's Early Innovations Provided a Glimpse of the Future," Natl. Geogr. Channel.

[2] Gopura, R. A. R. C., Bandara, D. S. V., Kiguchi, K., and Mann, G. K. I., 2016, "Developments in Hardware Systems of Active Upper-Limb Exoskeleton Robots: A Review," Rob. Auton. Syst., **75**, pp. 203–220.

[3] Sankai, Y., 2006, "Leading Edge of Cybernics: Robot Suit HAL," SICE-ICASE Int. Jt. Conf., **10**, pp. 1–2.

[4] Perry, J. C., Rosen, J., and Burns, S., 2007, "Upper-Limb Powered Exoskeleton Design," IEEE/ASME Trans. Mechatronics, **12**(4), pp. 408–417.

[5] Balasubramanian, S., Wei, H. R., Perez, M., Shepard, B., Koeneman, E., Koeneman, J., and He, J., 2008, "Rupert: An Exoskeleton Robot for Assisting Rehabilitation of Arm Functions," *Virtual Rehabilitation (IEEE)*, pp. 163–167.

[6] Dollar, A. M., and Herr, H., 2008, "Lower Extremity Exoskeletons and Active Orthoses : Challenges and State-of-the-Art," IEEE Trans. Robot., **24**(1), pp. 144–158.

[7] Herr, H., 2009, "Exoskeletons and Orthoses : Classification , Design Challenges and Future Directions," J. Neuroeng. Rehabil., **9**, pp. 1–9.

[8] Chu, A., Kazerooni, H., Zozz, A., Zoss, A. B., Kazerooni, H., and Chu, A., 2006, "On the Biomimetic Design of the Berkeley Lower Extremity Exoskeleton (BLEEX)," *International Conference on Intelligent Robots and Systems*, pp. 3132–3139.

[9] United States Census, 2010, "Americans with Disabilities: 2010," U.S. Dep.

Commer.

[10] Refour, E., Sebastian, B., and Ben-Tzvi, P., 2018, "Two-Digit Robotic Exoskeleton Glove Mechanism: Design and Integration," J. Mech. Robot., **10**(2), p. 025002.

[11] Refour, E., Sebastian, B., Chauhan, R., Ben-Tzvi, P., 2019, "A General Purpose Robotic Hand Exoskeleton with Series Elastic Actuators," J. Mech. Robot. Trans. ASME, p. Accepted.

[12] Ma, Z., and Ben-Tzvi, P., 2013, "Tendon Transmission Efficiency of a Two-Finger Haptic Glove," *2013 IEEE International Symposium on Robotic and Sensors Environments (ROSE)*, IEEE, pp. 13–18.

[13] Ho, N. S. K., Tong, K. Y., Hu, X. L., Fung, K. L., Wei, X. J., Rong, W., and Susanto, E. A., 2011, "An EMG-Driven Exoskeleton Hand Robotic Training Device on Chronic Stroke Subjects: Task Training System for Stroke Rehabilitation," IEEE Int. Conf. Rehabil. Robot.

[14] Worsnopp, T. T., Peshkin, M. A., Colgate, J. E., and Kamper, D. G., 2007, "An Actuated Finger Exoskeleton for Hand Rehabilitation Following Stroke," 2007 IEEE 10th Int. Conf. Rehabil. Robot. ICORR'07, **00**(c), pp. 896–901.

[15] Ertas, I. H., Hocaoglu, E., Barkana, D. E., and Patoglu, V., 2009, "Finger Exoskeleton for Treatment of Tendon Injuries," Proc. 11th IEEE Int. Conf. Rehabil. Robot. ICORR, pp. 194–201.

[16] Hasegawa, Y., Mikami, Y., Watanabe, K., and Sankai, Y., 2008, "Five-Fingered Assistive Hand with Mechanical Compliance of Human Finger," Proc. - IEEE Int. Conf. Robot. Autom., pp. 718–724.

[17] Zhou, M. A., Ben-Tzvi, P., and Danoff, J., 2015, "Hand Rehabilitation Learning System with an Exoskeleton Robotic Glove," IEEE Trans. Neural Syst. Rehabil. Eng., **PP**(99), pp. 1323–1332.

[18] Ben-Tzvi, P., Danoff, J., and Ma, Z., 2016, "The Design Evolution of a Sensing and Force-Feedback Exoskeleton Robotic Glove for Hand Rehabilitation Application," J. Mech. Robot., **8**(5), p. 051019.

[19] CyberGlove Systems LLC, 2009, "CyberGrasp."

[20] Ben-Tzvi, P., and Ma, Z., 2015, "Sensing and Force-Feedback Exoskeleton (SAFE) Robotic Glove," IEEE Trans. Neural Syst. Rehabil. Eng., **23**(6), pp. 992–1002.

[21] Arata, J., Ohmoto, K., Gassert, R., Lambercy, O., Fujimoto, H., and Wada, I., 2013, "A New Hand Exoskeleton Device for Rehabilitation Using a Three-Layered Sliding Spring Mechanism," Proc. - IEEE Int. Conf. Robot. Autom., pp. 3902–3907.

[22] Iqbal, J., Khan, H., Tsagarakis, N. G., and Caldwell, D. G., 2014, "ScienceDirect A Novel Exoskeleton Robotic System for Hand Rehabilitation – Conceptualization to Prototyping," Integr. Med. Res., **34**(2), pp. 79–89.

[23] In, H., and Cho, K., 2015, "Exo-Glove : Soft Wearable Robot for the Hand Using Soft Tendon Routing System," IEEE Robot. Autom., **22**(March 2015), pp. 97–105.

[24] Lee, S. W., Landers, K. A., and Park, H., 2014, "Development of a Biomimetic Hand Exotendon Device (BiomHED) for Restoration of Functional Hand Movement Post-Stroke," IEEE Trans. Neural Syst. Rehabil. Eng., **22**(4), pp. 886–898.

[25] Nycz, C. J., Delph, M. A., and Fischer, G. S., 2015, "Modeling and Design of a Tendon Actuated Soft Robotic Exoskeleton for Hemiparetic Upper Limb Rehabilitation," 2015 37th Annu. Int. Conf. IEEE Eng. Med. Biol. Soc., pp. 3889–3892.

[26] Hasegawa, Y., Tokita, J., Kamibayashi, K., and Sankai, Y., 2011, "Evaluation of Fingertip Force Accuracy in Different Support Conditions of Exoskeleton," Proc. - IEEE Int. Conf. Robot. Autom., pp. 680–685.

[27] Koo, I., Byunghyun Kang, B., and Cho, K.-J., 2013, "Development of Hand Exoskeleton Using Pneumatic Artificial Muscle Combined with Linkage," J. Korean Soc. Precis. Eng, **11**(11), pp. 1217–1224.

[28] Polygerinos, P., Wang, Z., Galloway, K. C., Wood, R. J., and Walsh, C. J., 2015, "Soft Robotic Glove for Combined Assistance and At-Home Rehabilitation," Rob. Auton. Syst., **73**, pp. 135–143.

[29] Polygerinos, P., Lyne, S., Wang, Z., Nicolini, L. F., Mosadegh, B., Whitesides, G. M., and Walsh, C. J., 2013, "Towards a Soft Pneumatic Glove for Hand Rehabilitation," IEEE Int. Conf. Intell. Robot. Syst., pp. 1512–1517.

[30] Yap, H. K., Lim, J. H., Nasrallah, F., Goh, J. C. H., and Yeow, R. C. H., 2015, "A Soft Exoskeleton for Hand Assistive and Rehabilitation Application Using Pneumatic Actuators with Variable Stiffness," *IEEE International Conference on Robotics and Automation (ICRA)*, pp. 4967–4972.

[31] Howard, W. S., and Kumar, V., 1996, "Vz 2 0," **12**(6), pp. 904–917.

[32] Nakashima, A., Yoshimastsu, Y., and Hayakawa, Y., 2010, "Analysis and Synthesis of Stable Grasp by Multi-Fingered Robot Hand," *IEEE International*

Conference on Control Application, pp. 1582–1589.

[33] Lu, Y., Zhang, C., Cao, C., and Liu, Y., 2017, "Analysis of Coordinated Grasping Kinematics and Optimization of Grasping Force of a Parallel Hybrid Hand," Int. J. Adv. Robot. Syst., **14**(3), pp. 1–14.

[34] Bekiroglu, Y., Laaksonen, J., Jørgensen, J., Kyrki, V., and Kragic, D., 2010, "Learning Grasp Stability Based on Haptic Data," Proc. RSS 2010 Work. Represent. object grasping Manip. single dual arm tasks.

[35] Kinoshita, H., Murase, T., and Bandou, T., 1996, "Grip Posture and Forces during Holding Cylindrical Objects with Circular Grips," Ergonomics, **39**(9), pp. 1163–1176.

[36] Dang, H., and Allen, P. K., 2012, "Learning Grasp Stability," Proc. - IEEE Int. Conf. Robot. Autom., pp. 2392–2397.

[37] Kragten, G. A., Baril, M., Gosselin, C., and Herder, J. L., 2011, "Stable Precision Grasps by Underactuated Grippers," IEEE Trans. Robot., **27**(6), pp. 1056–1066.

[38] Suhaib, M., Khan, R. A., and Mukherjee, S., 2011, "Contact Force Optimization For Stable Grasp Of Multifingire Robotic Grippers," World Congr. Eng., **III**, pp. 6–9.

[39] Haas-Heger, M., Iyengar, G., and Ciocarlie, M., 2018, "Passive Reaction Analysis for Grasp Stability," IEEE Trans. Autom. Sci. Eng., **15**(3), pp. 955–966.

[40] Lee, B. J. B., Williams, A., Ben-tzvi, P., and Member, S., 2018, "Intelligent Object Grasping With Sensor Fusion for Rehabilitation and Assistive Applications," IEEE Trans. Neural Syst. Rehabil. Eng., **26**(8), pp. 1556–1565.

[41] Chauhan, R. J., and Ben-Tzvi, P., 2018, "Latent Variable Grasp Prediction for

Exoskeletal Glove Control," *Proceedings of the ASME 2018 Dynamic Systems and Control Conf.*, p. V001T07A002.

[42] Chauhan, R., Sebastian, B., Ben-Tzvi, P., 2019, "Grasp Prediction Towards Naturalistic Exoskeleton Glove Control," IEEE Trans. Human-Machine Syst., p. Accepted.

[43] Howard, A. M., and Bekey, G. A., 2000, "Intelligent Learning for Deformable Object Manipulation," pp. 51–58.

[44] Cretu, A., Payeur, P., and Petriu, E. M., 2012, "Soft Object Deformation Monitoring and Learning for Model-Based Robotic Hand Manipulation," IEEE Trans. Syst. Man, Cybern. Part B, **42**(3), pp. 740–753.

[45] Drimus, A., Kootstra, G., Bilberg, A., and Kragic, D., 2011, "Classification of Rigid and Deformable Objects Using a Novel Tactile Sensor," 2011 15th Int. Conf. Adv. Robot., pp. 427–434.

[46] Khalil, F. F., Payeur, P., and Cretu, A., 2010, "INTEGRATED MULTISENSORY ROBOTIC HAND SYSTEM FOR DEFORMABLE OBJECT MANIPULATION," (Ra).

[47] Delgado, A., Jara, C. A., Mira, D., and Torres, F., 2015, "A Tactile-Based Grasping Strategy for Deformable Objects ' Manipulation and Deformability Estimation," 2015 12th Int. Conf. Informatics Control. Autom. Robot., **02**, pp. 369–374.

[48] Huang, J., Todo, I., and Yabuta, T., 2005, "Position / Force Hybrid Control of a Manipulator with a Flexible Tool Using Visual and Force Information," (July).

[49] Feix, T., Romero, J., Schmiedmayer, H.-B., Dollar, A. M., and Kragic, D., 2016,

"The GRASP Taxonomy of Human Grasp Types," IEEE Trans. Human-Machine Syst., **46**(1), pp. 66–77.

[50] Chauhan, R., Ben-Tzvi, P., 2019, "A Series Elastic Actuator Design and Control in a Linkage Based Hand Exoskeleton," *Proceedings of the ASME 2019 Dynamic Systems and Control Conf.*, Park City, Utah, p. Accepted.

[51] Dos Santos, W. M., and Siqueira, A. A. G., 2014, "Impedance Control of a Rotary Series Elastic Actuator for Knee Rehabilitation," IFAC Proc. Vol., **19**, pp. 4801–4806.

[52] Knox, B. T., and Schmiedeler, J. P., 2009, "A Unidirectional Series-Elastic Actuator Design Using a Spiral Torsion Spring," J. Mech. Des., **131**(12), p. 125001.

[53] S. Boyd and L. Vandenberghe, 2004, *Convex Optimization*, Cambridge, U.K.: Cambridge Univ. Press.

[54] Vanteddu, T., Sebastian, B., and Ben-Tzvi, P., 2018, "Design Optimization of RML Glove for Improved Grasp Performance," *Volume 1: Advances in Control Design Methods; Advances in Nonlinear Control; Advances in Robotics; Assistive and Rehabilitation Robotics; Automotive Dynamics and Emerging Powertrain Technologies; Automotive Systems; Bio Engineering Applications; Bio-Mecha*, ASME, Atlanta, GA, p. V001T07A004.